The Astrophysical Journal Supplement Series, 269:32 (23pp), 2023 November https://doi.org/10.3847/1538-4365/acfbe4

The GW Vir Instability Strip in Light of New Observations of PG 1159 Stars: Discovery of Pulsations in the Central Star of A72 and Variability of RX J0122.9–7521

Paulina Sowicka[1], Gerald Handler[1], David Jones[2,3,4], John A. R. Caldwell[5], Francois van Wyk[6], Ernst Paunzen[7], Karolina Bąkowska[8], Luis Peralta de Arriba[9,10], Lucía Suárez-Andrés[10], Klaus Werner[11], Marie Karjalainen[12], and Daniel L. Holdsworth[13]

[1] Nicolaus Copernicus Astronomical Center, Polish Academy of Sciences, ul. Bartycka 18, PL-00-716, Warszawa, Poland; paula@camk.edu.pl, gerald@camk.edu.pl
[2] Instituto de Astrofísica de Canarias, E-38205 La Laguna, Tenerife, Spain
[3] Departamento de Astrofísica, Universidad de La Laguna, E-38206 La Laguna, Tenerife, Spain
[4] Nordic Optical Telescope, Rambla José Ana Fernández Pérez 7, E-38711, Breña Baja, Spain
[5] McDonald Observatory, 82 Mt. Locke Road, TX 79734, USA
[6] South African Astronomical Observatory, P.O. Box 9, Observatory, 7935 Cape Town, South Africa
[7] Department of Theoretical Physics and Astrophysics, Faculty of Science, Masaryk University, Kotlářská 2, Brno, Czech Republic
[8] Institute of Astronomy, Faculty of Physics, Astronomy and Informatics, Nicolaus Copernicus University, ul. Grudziądzka 5, 87-100 Toruń, Poland
[9] Centro de Astrobiología (CAB), CSIC-INTA, Camino Bajo del Castillo s/n, E-28692 Villanueva de la Cañada, Madrid, Spain
[10] Isaac Newton Group of Telescopes, E-38700 Santa Cruz de La Palma, La Palma, Spain
[11] Institut für Astronomie und Astrophysik, Kepler Center for Astro and Particle Physics, Eberhard Karls Universität, Sand 1, D-72076 Tübingen, Germany
[12] Astronomical Institute, Czech Academy of Sciences, Fričova 298, 25165, Ondřejov, Czech Republic
[13] Jeremiah Horrocks Institute, University of Central Lancashire, Preston, PR1 2HE, UK
Received 2023 July 31; revised 2023 September 8; accepted 2023 September 19; published 2023 November 10

Abstract

We present the results of new time-series photometric observations of 29 pre–white dwarf stars of PG 1159 spectral type, carried out in the years 2014–2022. For the majority of stars, a median noise level in Fourier amplitude spectra of 0.5–1.0 mmag was achieved. This allowed the detection of pulsations in the central star of planetary nebula A72 (Abell 72), consistent with *g* modes excited in GW Vir stars, and variability in RX J0122.9–7521 that could be due to pulsations, binarity, or rotation. For the remaining stars from the sample that were not observed to vary, we placed upper limits for variability. After combination with literature data, our results place the fraction of pulsating PG 1159 stars within the GW Vir instability strip at 36%. An updated list of all known PG 1159 stars is provided, containing astrometric measurements from the recent Gaia DR3 data, as well as information on physical parameters, variability, and nitrogen content. Those data are used to calculate luminosities for all PG 1159 stars to place the whole sample on the theoretical Hertzsprung–Russell diagram for the first time in that way. The pulsating stars are discussed as a group, and arguments are given that the traditional separation of GW Vir pulsators in "DOV" and "PNNV" stars is misleading and should not be used.

Unified Astronomy Thesaurus concepts: PG 1159 stars (1216); Pulsating variable stars (1307); Stellar pulsations (1625); Non-radial pulsations (1117); Stellar evolution (1599); CCD photometry (208); Hertzsprung Russell diagram (725); Post-asymptotic giant branch stars (2121); Instability strip (798)

1. Introduction

Pre–white dwarf (WD) stars of PG 1159 spectral type (named after the prototype, PG 1159–035; Green & Liebert 1979) are important to study in the context of stellar evolution, as they are supposed main progenitors of H-deficient WDs. PG 1159 stars populate the GW Vir instability strip, together with central stars of planetary nebulae with C-rich Wolf–Rayet spectra ([WC] types, exhibiting He, C, and O lines in emission; Crowther et al. 1998) and [WC]-PG 1159 stars, so-called transition objects (Leuenhagen et al. 1993; Toalá et al. 2015). PG 1159 stars exhibit a broad absorption "trough" made by He II at 4686 Å and adjacent C IV lines (see, e.g., Figure 2 in Werner & Rauch 2014) and typically have He-, C-, and O-rich atmospheres, but notable variations in He, C, and O abundances were found from star to star (e.g., Dreizler & Heber 1998; Werner 2001). Other groups of (pre-)WD stars also show He II and C IV lines—while the O(He) stars show significantly less carbon than PG 1159 stars (up to 3% in their atmospheres; Reindl et al. 2014), the limit to distinguish between PG 1159 stars and DO WDs is model dependent—Werner et al. (2014) adopted C/He up to 9% (by mass) for DO stars.

Their formation history involves either a single-star evolution scenario—a "born-again" episode (a very late thermal pulse (VLTP) or a late thermal pulse (LTP); PG 1159-hybrid stars experience an AGB final thermal pulse)—or binary evolution–binary WD merger (Werner et al. 2022b; Miller Bertolami et al. 2022). Only some stars within the GW Vir instability strip show pulsations, a striking difference from the other two classical WD instability strips (DAV and DBV), which are believed to be pure (see, e.g., Fontaine & Brassard 2008). The GW Vir pulsations are due to nonradial *g* modes, where the main restoring force is gravity (buoyancy), driven by the $\kappa - \gamma$ mechanism associated with the partial ionization of the K-shell electrons of carbon and/or oxygen in the envelope. The pulsations typically are of short period (between 300 and about 6000 s) and low amplitude (typically 1 mmag–0.15 mag; Córsico et al. 2019).

A current hypothesis, based on combined photometric and spectroscopic observations, states that there is a clear separation

within PG 1159 stars: all N-rich (about 1% atmospheric N/He abundance) PG 1159 stars are pulsators, while all N-poor ones (below about 0.01% N/He) do not pulsate (Dreizler & Heber 1998; Sowicka et al. 2021). Since N is a tracer of the evolutionary history, an important conclusion follows: the pulsating and nonpulsating PG 1159 stars have different evolutionary histories, and it seems necessary that a star undergoes a VLTP in order to develop pulsations. Recently, considerable progress has been made in the study of PG 1159 stars' atmospheric structure, composition, and evolution through optical and ultraviolet spectroscopy and advancement in non-LTE model atmospheres, as well as in probing their interiors through asteroseismology with space-based observations (e.g., the TESS mission (Ricker et al. 2015) observed several already-known GW Vir stars; Córsico et al. 2021). In light of these findings, it is important to further test this hypothesis on a larger sample of PG 1159 stars, by obtaining high-quality, high-speed photometric observations aimed at detecting low-amplitude pulsations if present, as well as spectroscopic observations capable of detecting the nitrogen lines.

The number of known PG 1159 stars has increased in recent years, due to both the detection of pulsations typical for GW Vir stars in new photometric surveys (e.g., TESS; Uzundag et al. (2021, 2022); confirmed by spectroscopy) and classification of targets of spectroscopic surveys (e.g., the most recent discoveries with HET; Bond et al. 2023). Currently, 67 PG 1159 stars are known,[14] including hybrid-PG 1159 stars (whose atmospheres have traces of hydrogen). While these stars lay within the GW Vir instability strip, either some of them were never checked for (or reported) variability, or the quality of previous observations was not sufficient to detect low-amplitude pulsations. They also could have been observed when beating between closely spaced modes was destructive and pushed the observed amplitudes below the detection threshold. Moreover, some of these objects have temporally highly variable pulsation spectra (Ciardullo & Bond 1996). Therefore, it is worth reobserving those stars in different observing cycles to look for photometric variability. To date, there has been no extensive and systematic photometric survey for variability among those stars since the works of Grauer et al. (1987b), Ciardullo & Bond (1996), and González Pérez et al. (2006).

The aim of the work presented in this paper is to obtain new photometric observations of a selected sample of PG 1159 stars to find new pulsators (or candidates) and put limits on nonvariability. We also provide the most up-to-date list of PG 1159 stars and their properties from the Gaia mission and follow-up works. Finally, we place the PG 1159 stars on the theoretical Hertzsprung–Russell (H-R) diagram ($\log L_\star/L_\odot - \log T_{\rm eff}$) and discuss the implications of our findings.

2. Photometric Observations

We selected a sample of PG 1159 stars for a survey of variability carried out in the years 2014–2022 with a network of telescopes, covering both hemispheres. The selection was based on only one criterion: a given star was included in our target list if it was never observed photometrically with time resolution sufficient for the detection of GW Vir pulsations, or was classified as nonvariable, but the reported detection limits either could have been improved by new observations or were not provided by the previous authors. The top panel of Figure 1 shows the brightness distribution of observed stars. The observing plan assumed the acquisition of observing blocks lasting at least 1 hr per target. The following telescopes and instruments were used for observations:

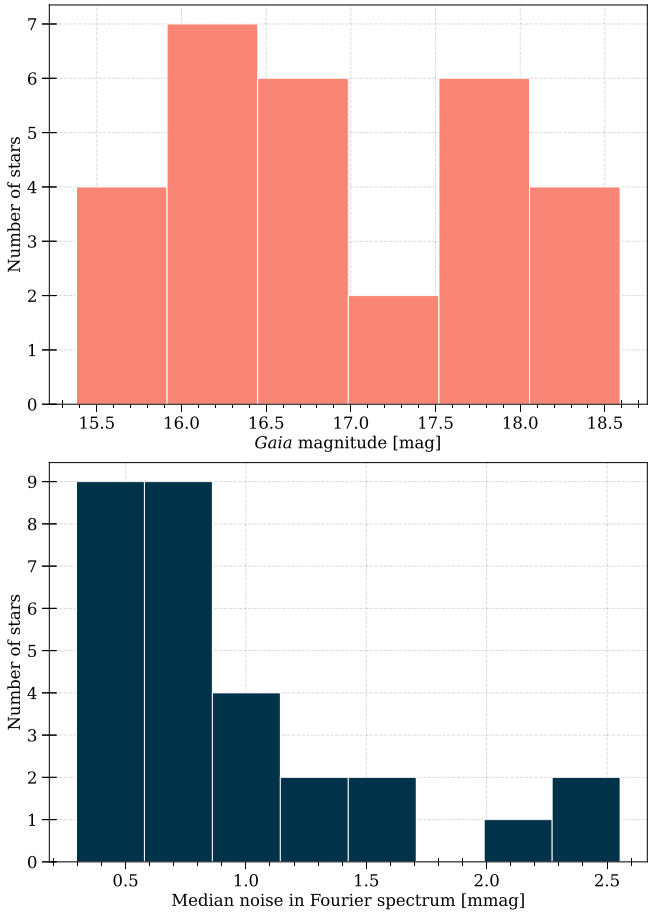

Figure 1. Top: Gaia magnitude distribution of the observed sample of 29 PG 1159 stars. Bottom: distribution of the median noise level achieved in the survey.

1. *DFOSC at the 1.54 m Danish Telescope at ESO (DK).* The 1.54 m Danish Telescope located at La Silla Observatory was equipped with the Danish Faint Object Spectrograph and Camera (DFOSC; Andersen et al. 1995). DFOSC uses a 2k × 2k thinned Loral CCD chip with a field of view (FOV) of 13.′7 × 13.′7. No filter was used. Six stars were observed with this telescope.
2. *OSIRIS at 10.4 m Gran Telescopio Canarias (GTC).* The 10.4 m GTC is located at the Observatorio del Roque de los Muchachos (La Palma) and is equipped with Optical System for Imaging and low-Intermediate-Resolution Integrated Spectroscopy (OSIRIS; Cepa 1998). OSIRIS consists of a mosaic of two CCDs of 2048 × 4096 pixels each and has an unvignetted FOV of 7.′8 × 7.′8. Either no filter or a Sloan *r*' filter was used. We used 2 × 2 binning and a standard readout time of about 23 s. Eleven stars were observed with this telescope.
3. *WFC at 2.54 m Isaac Newton Telescope (INT).* The 2.54 m Isaac Newton Telescope (INT) is located at the Observatorio del Roque de los Muchachos (La Palma) and is equipped with the Wide Field Camera (WFC; Walton et al. 2001), an optical mosaic camera mounted in the prime focus. WFC consists of four thinned EEV

[14] Based on a list from Werner & Herwig (2006), updated by us.

2k × 4k CCDs. Because the readout time of the whole CCD mosaic is rather long, we used it in windowing mode—for an FOV of $5 \times 5'$ (910×910 pixels) the readout time was 6 s in the slow (less noisy) mode. No binning was used. We used a Harris V filter. Five stars were observed with this telescope.

4. *ProEM at the 2.1 m Otto Struve Telescope (MD).* The 2.1 m Otto Struve Telescope is located at McDonald Observatory and is equipped with ProEM, which is a frame-transfer CCD detector with optional electron multiplication with high frame rate, optimized for high-speed time-series photometry (providing effectively zero readout time). The CCD has 1024 × 1024 pixels and an FOV of $1\farcm6 \times 1\farcm6$. We used 4×4 binning for an effective plate scale of $0\farcs36$ pixel^{-1}. We used a BG40 filter. Nine stars were observed with this telescope.
5. *Andor at the 1.3 m McGraw-Hill Telescope (MDM).* The 1.3 m McGraw-Hill Telescope is located at the MDM Observatory, on the southwest ridge of Kitt Peak in Arizona. It was equipped with the Andor Ikon DU937_BV CCD camera, which was used in frame-transfer mode and 4×4 binning. We used a BG38 filter. One star was observed with this telescope.
6. *SHOC at the SAAO 1.9 m Telescope and 1.0 m Telescope (SA19, SA10).* The telescopes are located at the Sutherland station of the South African Astronomical Observatory (SAAO) and are equipped with one of the Sutherland High Speed Optical Cameras (SHOC; Coppejans et al. 2013). SHOC 1 and 2 are high-speed cameras operating in frame-transfer mode for visible wavelength range that have an electron-multiplying (EM) capability.[15] The imaging area of the detectors is 1024 × 1024 pixels, which corresponds to an FOV of $2\farcm79 \times 2\farcm79$ for the 1.9 m telescope with the focal reducer and $2\farcm85 \times 2\farcm85$ for the 1.0 m telescope. A selection of amplifiers can be used, each resulting in a different gain setting, as well as binning and readout speed. The slowest readout speed was usually chosen, resulting in the lowest readout noise. Binning was determined by the observer to match the observing conditions and especially avoid undersampling of the point-spread function. Observations were done without a filter. Four stars were observed with these telescopes.

The data were reduced using the following procedures. For data from DK we applied standard IRAF routines for all reduction steps. We extracted bad columns and hot pixels from the night's bias frames and flat fields and then cleaned the images for bad and hot pixels after the basic reduction steps (bias subtraction, dark and flat correction). As the last step, we checked for intensity gradients in the x- and y-directions (which sometimes occur in the presence of a bright Moon) and removed them, if necessary. The data from all the other instruments were reduced using standard `Astropy` (Astropy Collaboration et al. 2013, 2018) `ccdproc` (Craig et al. 2017) routines consisting of bias subtraction, dark correction (only for observations with ProEM), flat-field correction, and gain correction. Then, we performed aperture photometry using our own photometry pipeline with the use of adaptive circular apertures with sizes scaled to the seeing conditions for each frame (Sowicka et al. 2018, 2021) with a scaling factor determined for each star and run. Comparison stars were chosen (wherever possible) such that they were brighter than the target and close to it, isolated and outside any faint nebulae, and when the target was the brightest in the field, an "artificial" comparison star comprising the summed flux from up to three available comparison stars was used. Because our target stars usually are much hotter than the available comparison stars, the differential light curves were corrected for differential color extinction by fitting a straight line to a Bouguer plot (differential magnitude vs. air mass). In the final step, we cleaned the light curves by removing outliers (3.5σ clipping) and parts of data with bad quality (e.g., observations through thick clouds). We also inspected our differential magnitudes plotted against FWHM measurements to make sure that there is no correlation introduced by our photometry procedure. The constancy of the comparison stars was checked by examining differential light curves when more than one comparison star could be used. In the case of fields with only a single comparison star, we looked up their Gaia $G_{\rm BP} - G_{\rm RP}$ colors, transformed these to $V - I_c$,[16] and transformed those to $B - V$ (Caldwell et al. 1993). In that way, and with a rough correction for interstellar reddening, we inferred that none of the single comparison stars had $(B - V)_0 < 0.7$ and hence none of them lie in a κ-driven instability strip.

In this work, we present the results for a sample of 29 PG 1159 stars that are not surrounded by bright planetary nebulae. The list of targets, observing log, and information on the scaling factor used in the photometry procedure are given in Table 1. The light curves are presented in Figure 2.

3. Frequency Analysis

The light curves prepared in the previous step were the subject of frequency analysis. We used `Period04` (Lenz & Breger 2005) to calculate Fourier amplitude spectra for each star and run separately, up to the corresponding Nyquist frequency. The Fourier amplitude spectra are shown in Figure 2. The frequency range to which our survey is sensitive varies from star to star. The length of observations varied from slightly below an hour to a few hours, resulting in poor frequency resolution for the shortest ones (based on the Loumos & Deeming (1978) criterion of $\Delta f = 1.0/\Delta T$ for only the detection of modes[17]). For each Fourier amplitude spectrum, we calculated the median noise level, as well as our detection threshold (dashed line in Figure 2), adopted as an amplitude ratio of S/N $\geqslant 4$ (Breger et al. 1993). Table 1 includes the length of observations, corresponding frequency resolution, and median noise level in the Fourier spectra for all observed targets.

4. Survey Results

The bottom panel of Figure 1 presents a histogram of the number of stars versus the median noise level in the Fourier spectrum. In cases when the same star was observed multiple times, the lowest achieved level was taken. For the majority of observed stars, we reached a noise level of about 1 mmag or below. Grauer et al. (1987b) and Ciardullo & Bond (1996) reported their threshold for nonvariable targets as the maximum

[15] The EM mode has not been used for observations presented in this work.

[16] https://gea.esac.esa.int/archive/documentation/GDR3/Data_processing/chap_cu5pho/cu5pho_sec_photSystem/cu5pho_ssec_photRelations.html

[17] We note that for a correct determination of amplitudes and phases the criterion is $\Delta f > 1.5/\Delta T$.

Table 1
Log of Photometric Observations

Name	Equip.	Observer	Date +UTC Start	Filter	t_{exp} (s)	Scale Factor	ΔT	Δf (day^{-1})	Med. Noise (mmag)
BMP 0739–1418	DK	EP	2014-12-26T05:48:30	no filter	30	1.5	2.39 hr	10.06	0.31
H1504+65	GTC	SA	2016-03-09T02:07:53	Sloan *r*	6	1.5	48 minutes	30.00	0.42
HS 0444+0453	DK	EP	2014-12-26T03:44:44	no filter	20	1.2	1.81 hr	13.24	0.52
HS 0704+6153	GTC	SA	2016-03-09T22:30:36	Sloan *r*	10	1.5	48 minutes	30.34	0.53
HS 1517+7403	MD	GH	2016-05-24T02:59:58	BG40	10	0.9	1.51 hr	15.88	0.61
MCT 0130–1937	SA19	PS	2014-12-05T19:15:59	no filter	10	0.9	2.30 hr	10.45	0.83
PG 1151–029	INT	NH	2016-03-29T21:44:06	Harris *V*	10	1.5	1.45 hr	16.61	0.57
PG 1520+525	MD	GH	2016-05-30T02:47:51	BG40	15	1.2	1.15 hr	20.87	0.66
PN A66 (Abell) 21	DK	EP	2015-02-10T02:01:46	no filter	40	1.2	1.16 hr	20.71	2.02
	GTC	SA	2016-03-08T22:26:12	Sloan *r*	6	1.2	50 minutes	29.04	0.44
PN A66 (Abell) 72	SA10	FW	2022-10-07T18:35:41	no filter	25	1.8	3.05 hr	7.87	1.29
			2022-10-08T18:01:35	no filter	30-35	1.5	2.04 hr	11.76	1.58
PN IsWe 1	INT	MK+Students	2016-10-19T04:11:53	Harris *V*	5	0.9	1.94 hr	12.40	0.81
PN Jn 1	INT	LSA, PSh	2016-12-12T20:47:54	Harris *V*	10	1.2	3.01 hr	7.98	0.81
	MD	JC	2017-08-16T07:54:09	BG40	10	1.2	3.75 hr	6.40	0.30
	MD	JC	2017-08-17T09:37:05	BG40	10	1.2	1.93 hr	12.41	0.35
	INT	DJ	2017-08-28T01:45:39	Harris *V*	5	1.5	3.71 hr	6.47	0.41
	INT	DJ	2017-08-30T03:03:13	Harris *V*	10	1.2	2.64 hr	9.09	0.45
PN Lo (Longmore) 3	DK	EP	2015-02-10T00:41:13	no filter	40	1.2	1.16 hr	20.65	2.40
RX J0122.9–7521	SA19	PS	2014-12-04T19:05:30	no filter	10	0.9	1.95 hr	12.32	0.49
			2014-12-09T18:32:43	no filter	10	0.9	2.42 hr	9.92	0.46
SDSS J000945.46+135814.4	GTC	SA	2017-12-06T22:18:56	no filter	10	1.2	58 minutes	24.63	2.55
SDSS J001651.42–011329.3	SA19	PS	2017-12-06T22:18:55	Sloan *r*	20	0.9	1.71 hr	14.04	1.58
SDSS J055905.02+633448.4	GTC	SA	2017-09-15T04:09:52	Sloan *r*	20	1.2	59 minutes	24.43	0.98
SDSS J075540.94+400918.0	GTC	SA	2016-03-06T23:31:33	Sloan *r*	15	1.2	57 minutes	25.21	0.59
SDSS J093546.53+110529.0	DK	EP	2015-01-02T06:26:02	no filter	30	0.9	1.55 hr	15.45	1.37
	MD	JC	2017-05-06T03:00:17	BG40	30	1.2	2.92 hr	8.23	1.85
	GTC	SA	2018-08-14T14:45:58	Sloan *r*	20	1.2	57 minutes	25.05	0.86
SDSS J102327.41+535258.7	INT	LPA	2016-02-03T02:40:54	Harris *V*	20	1.2	2.52 hr	9.54	1.58
SDSS J105300.24+174932.9	MD	JC	2017-05-02T03:34:16	BG40	20	0.9	2.27 hr	10.56	0.78
	MD	JC	2017-05-07T03:08:52	BG40	22	0.9	3.04 hr	7.89	1.91
	GTC	SA	2017-12-29T02:27:34	Sloan *r*	10	1.2	1.05 hr	22.96	0.57
	MDM	KB	2019-04-24T04:19:17	BG38	30	1.5	1.99 hr	12.09	0.79
	MDM	KB	2019-04-25T03:36:34	BG38	30	1.2	1.82 hr	13.20	1.55
	MDM	KB	2019-04-26T02:54:19	BG38	30	1.2	4.00 hr	6.01	1.11
SDSS J121523.09+120300.8	DK	EP	2015-04-14T02:32:52	no filter	40	0.9	1.26 hr	19.04	2.97
	GTC	SA	2018-01-17T06:01:53	Sloan *r*	20	1.2	1.13 hr	21.17	0.95
SDSS J123930.61+244321.7	INT	PS, MT	2016-03-11T00:46:00	Harris *V*	20	0.9	2.10 hr	11.42	1.24
SDSS J134341.88+670154.5	MD	GH	2016-05-26T02:57:55	BG40	20	1.5	59 minutes	24.56	1.11
			2016-05-29T02:47:32	BG40	20	1.2	1.50 hr	16.00	0.92
SDSS J141556.26+061822.5	MD	JC	2017-05-05T05:14:23	BG40	30	1.2	5.20 hr	4.62	0.69
SDSS J144734.12+572053.1	MD	GH	2016-05-28T02:46:07	BG40	30	1.2	1.59 hr	15.08	2.25
SDSS J191845.01+624343.7	MD	JC	2017-05-08T07:08:02	BG40	30	0.9	4.15 hr	5.78	1.05
Sh 2–68	GTC	SA	2016-04-23T04:45:44	Sloan *r*	10	1.5	58 minutes	24.81	0.58
Sh 2–78	GTC	SA	2016-04-24T04:27:31	Sloan *r*	15	1.2	1.24 hr	19.30	0.75

Note. SA—support astronomer; students—Rosa Clavero, Francisco Galindo, Bartosz Gauza; GTC—GTC+OSIRIS; DK—DK154+DFOSC; MD—McDonald 2.1 m+ProEM; MDM—MDM 1.3 m+Andor; SA19—SAAO 1.9 m+SHOC; SA10—SAAO 1.0 m+SHOC; INT—INT+WFC. We refer to the central stars using the PN designations throughout the paper.

amplitude in the Fourier spectra and reached values of 2.4–2.7 mmag and 2.4–5.3 mmag, respectively. Inspection of Figure 2 shows that our results are comparable to theirs, while our sample covered fainter stars (15.4–18.6 mag in Gaia; see the top panel of Figure 1). This allowed us to discover pulsations in the central star of planetary nebula A72 and variability in RX

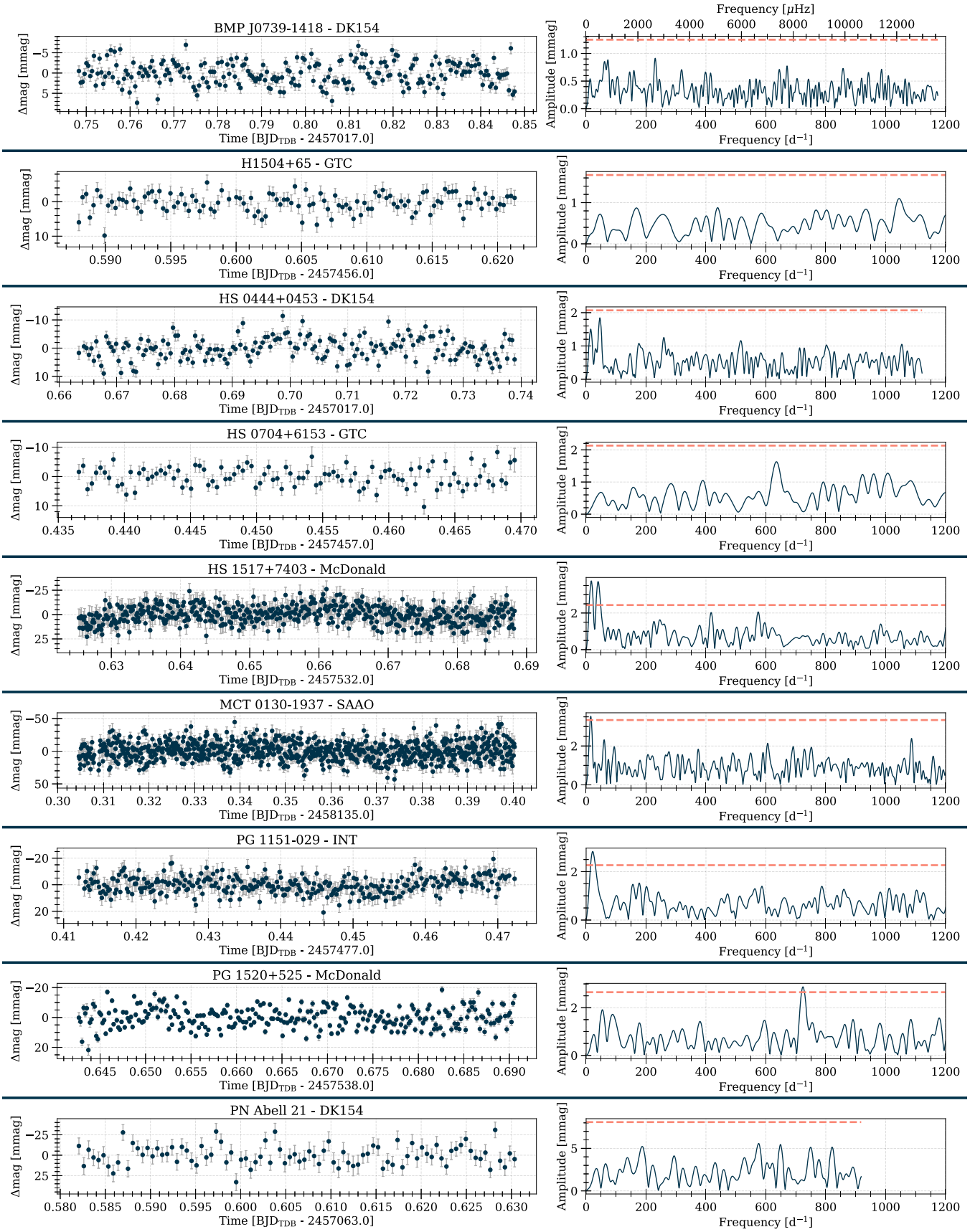

Figure 2. Light curves and their respective Fourier amplitude spectra of the survey targets. Plots for different stars are separated with horizontal lines. Light curves: note different scales. Fourier spectra: they were calculated up to their respective Nyquist frequencies but are plotted until 1200 day^{-1}. Dashed lines show the detection threshold of S/N $\geqslant$4. Note different scales.

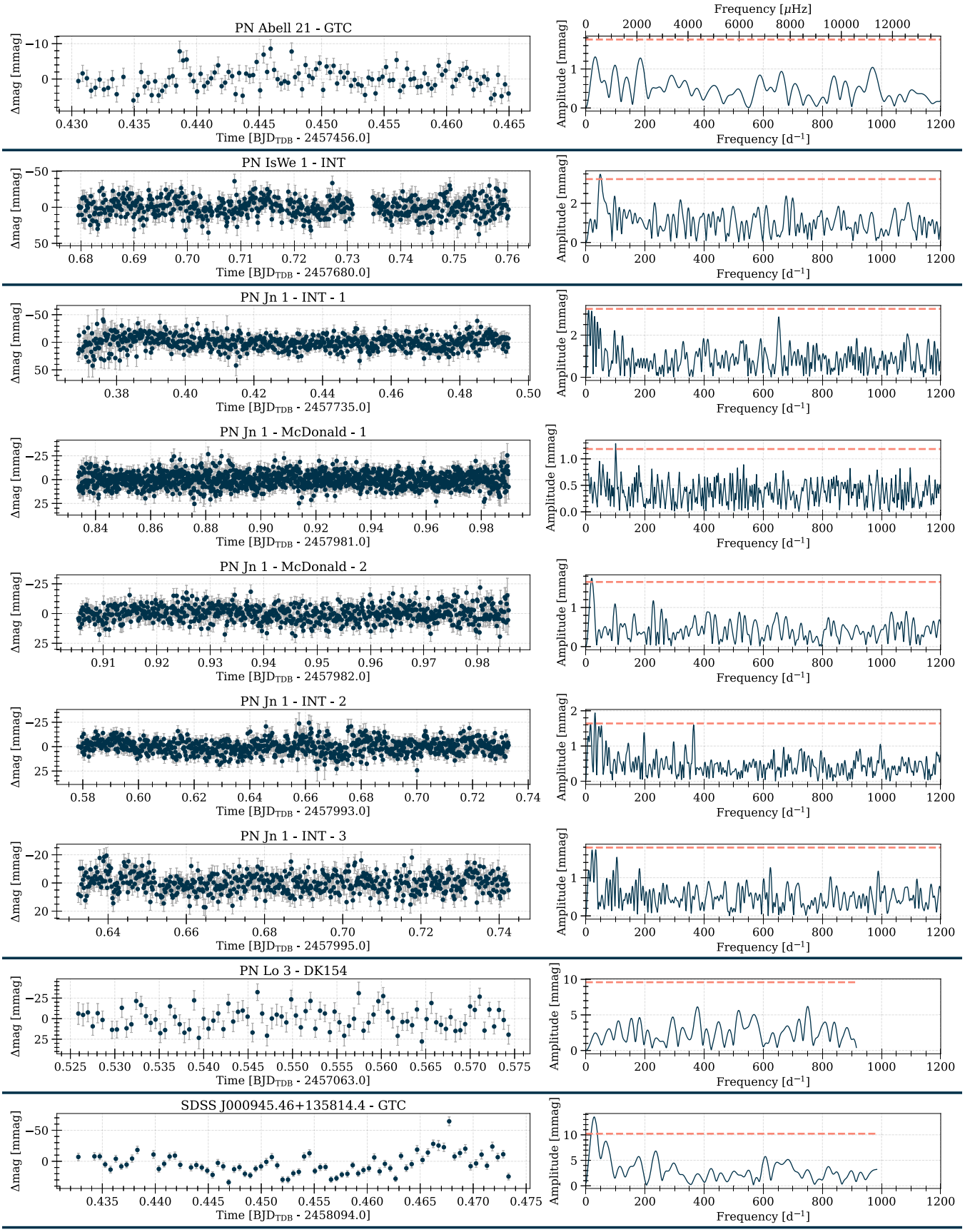

Figure 2. (Continued.)

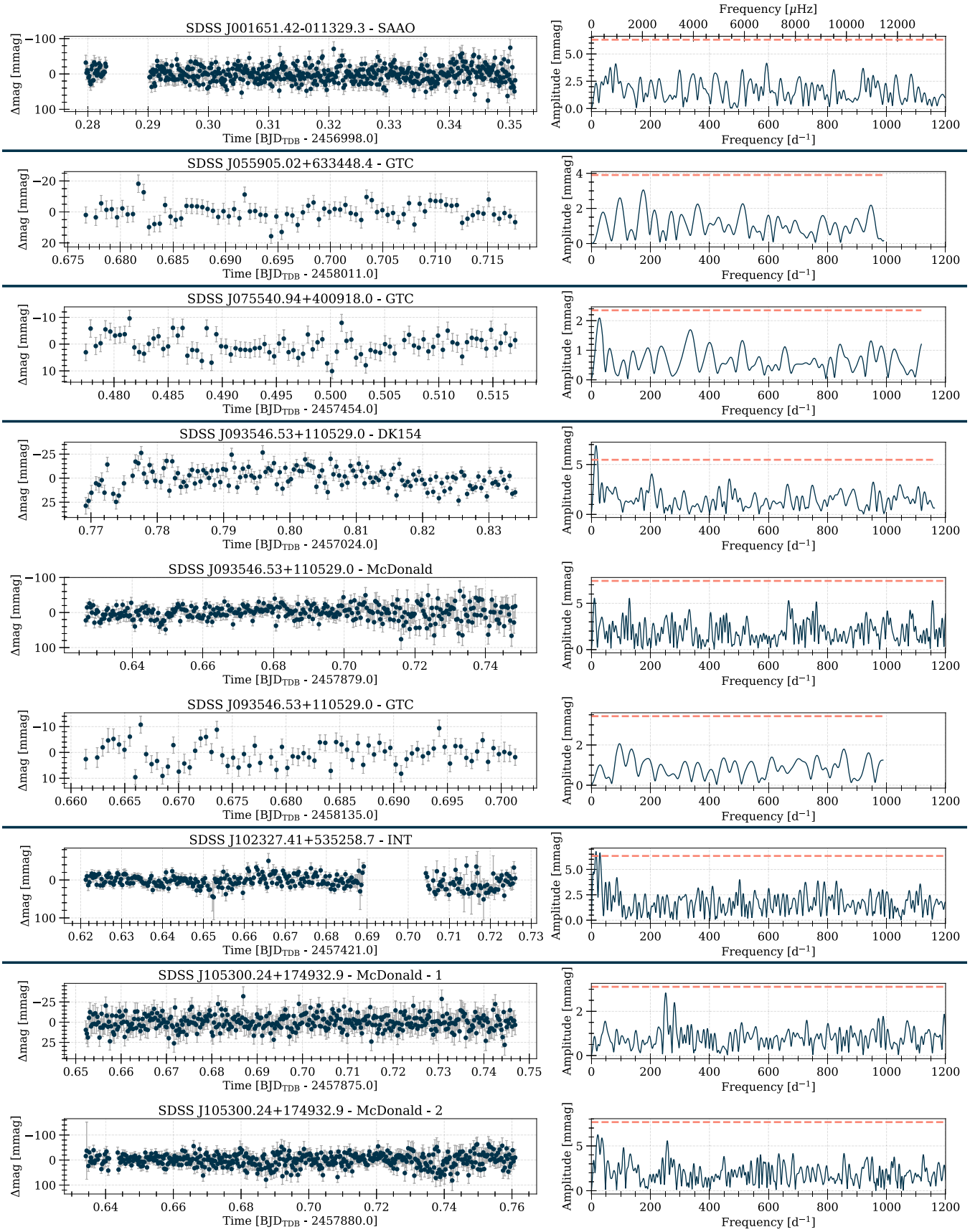

Figure 2. (Continued.)

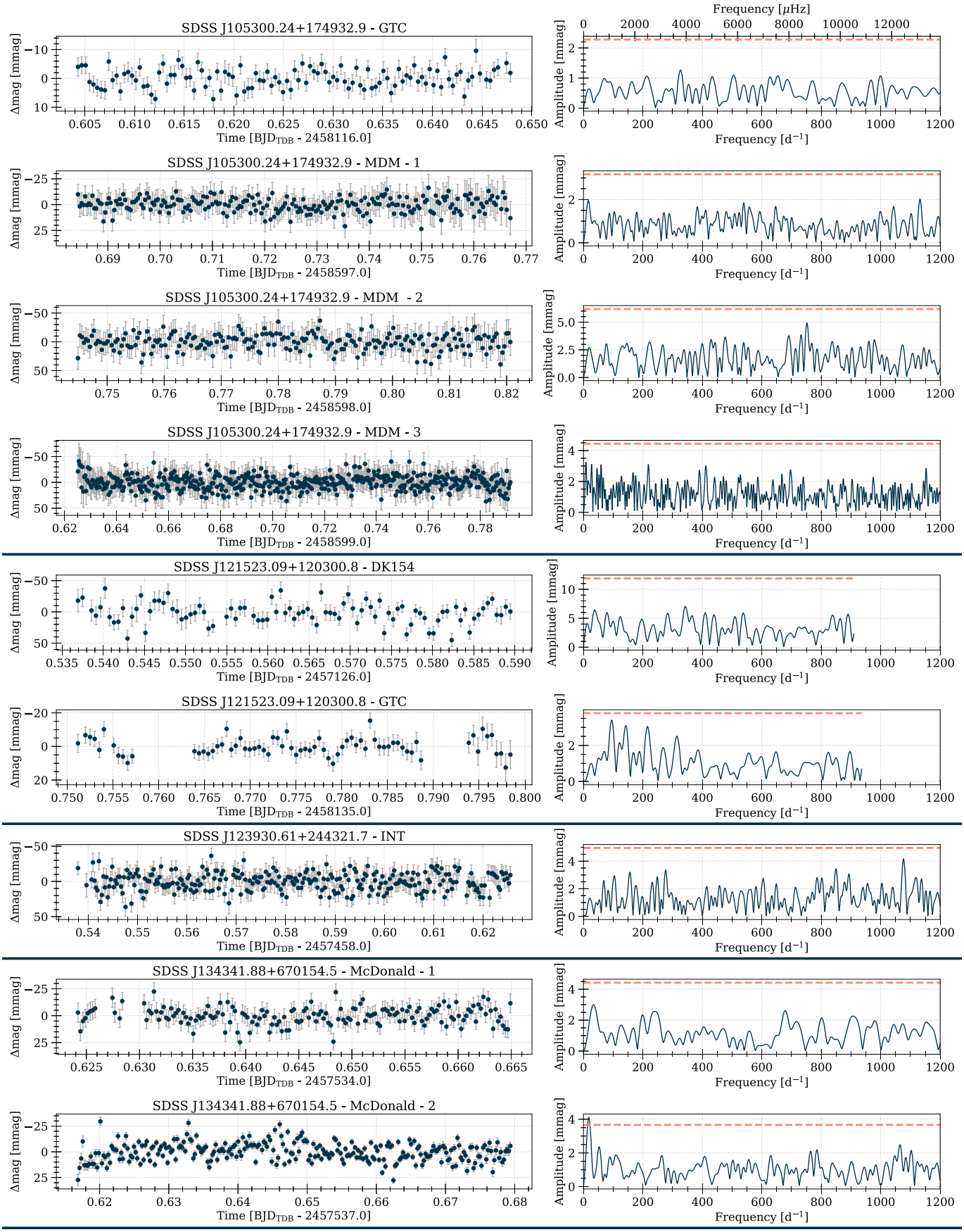

Figure 2. (Continued.)

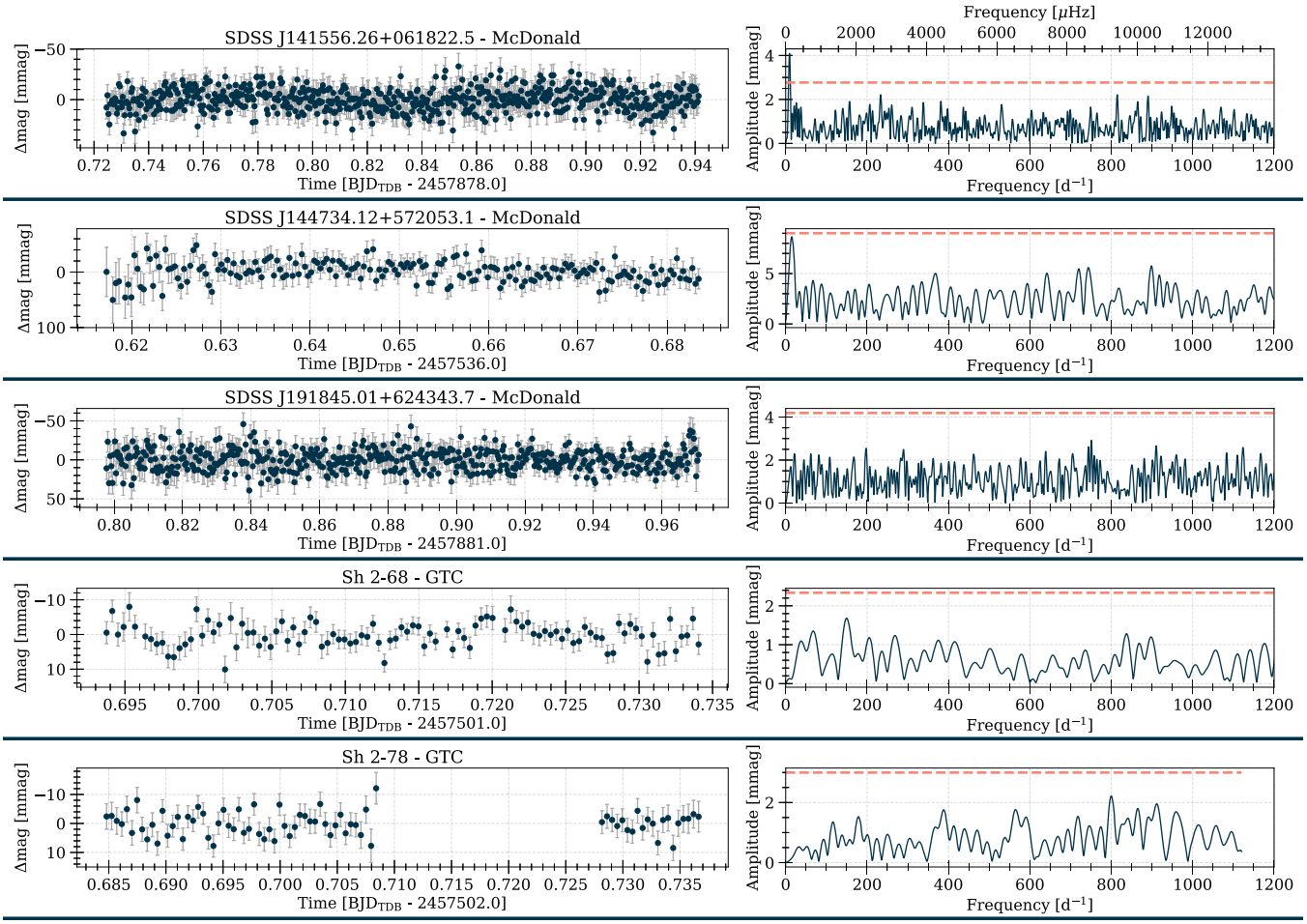

Figure 2. (Continued.)

J0122.9–7521. In addition to that, five objects from our sample could also be variable but need follow-up observations for eventual confirmation. The majority of our sample did not show any variability consistent with GW Vir pulsations, and in those cases we put upper limits on nonvariability. Each Fourier spectrum was also inspected for the presence of short-period ϵ-driven modes (Córsico et al. 2009). No sign of such modes with periods shorter than about 200 s (frequencies above 400 day^{-1}) was found in any of the stars.

5. Comments on Selected Stars

Below, we comment on stars that showed peaks of interest in the Fourier spectrum. While most of our observations turned out to be nondetections, we have to mention one caveat. Pulsating PG 1159 stars are known for their variable pulsation spectra, even on a night-to-night basis. This is often caused by the interference between closely spaced modes, which occasionally becomes destructive and pushes the amplitudes of the modes below the detection threshold. Possible nonlinear mode coupling could have the same effect (e.g., Vauclair et al. 2011). Nondetections for those reasons could be avoided by observing the targets on multiple nights over the visibility period. While this was the case for eight targets, we were not able to acquire multiple runs for the remaining sample, and this has to be kept in mind regarding our nondetections.

5.1. Pulsator—PN A72

The central star of the planetary nebula A72 was observed in 2022 October over two consecutive nights. The light curves and Fourier amplitude spectra are presented in Figure 3. We detected significant peaks reaching amplitudes on the order of 10 mmag in the nightly Fourier amplitude spectra, on both nights located in the same frequency range, consistent with g-mode pulsations seen in GW Vir stars. We classify A72 as a multiperiodic pulsator, and observations on a longer time base are needed to resolve its pulsation modes.[18]

5.2. Candidates

1. *HS 0444+0453*. There is an interesting, but statistically insignificant (S/N = 3.3), peak around 45.7 day^{-1} (period of about 1890 s). If confirmed, it fits within the observed period range of GW Vir pulsators.
2. *HS 1517+7403*. There are two statistically significant peaks: 17.5 and 40.5 day^{-1} (S/N = 5.8 for both, periods of 4945 and 2133 s, respectively). Such long periods are usually found in GW Vir central stars of planetary nebulae, but no nebula around HS 1517+7403 has been reported. Given the short duration of the single run available and that only a single comparison star could be

[18] We refer to the central stars using the PN designations throughout the paper.

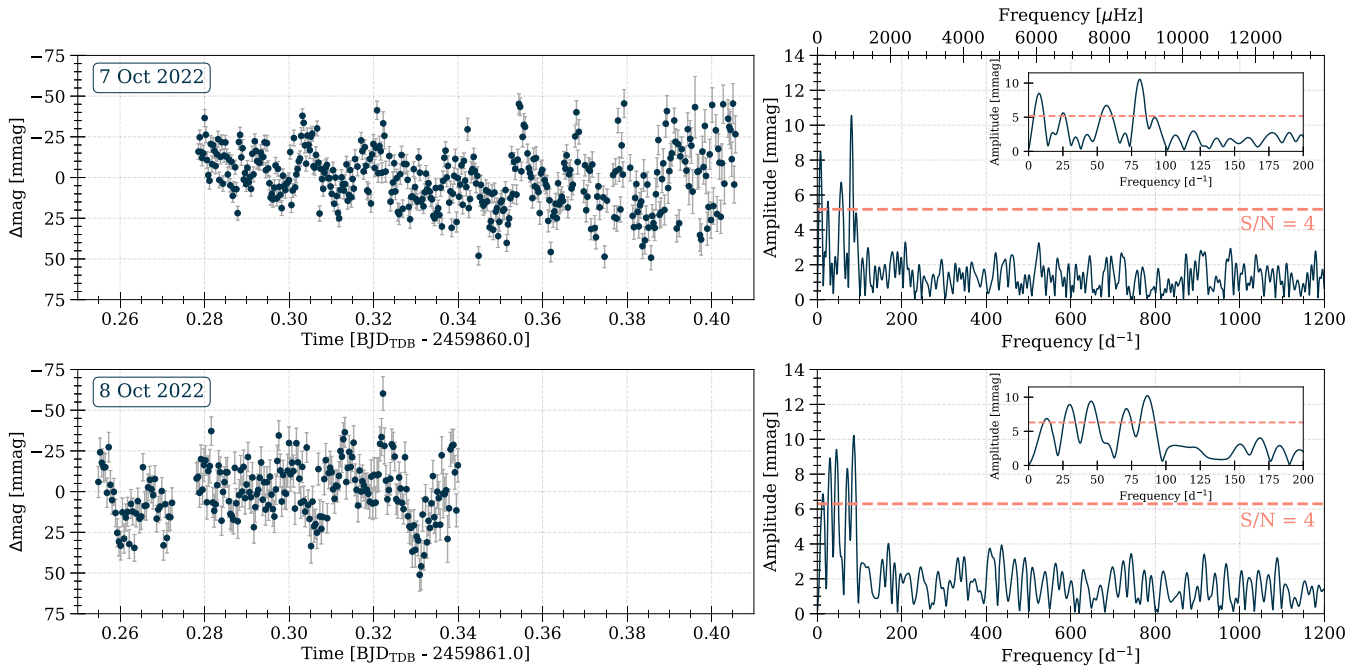

Figure 3. Light curves and Fourier amplitude spectra of two SAAO observing runs on the central star of planetary nebula A72. The Fourier amplitude spectra were calculated up to the Nyquist frequency but are shown up to 1200 day^{-1}. Insets show a zoomed-in view into the frequency range of detected pulsations. Dashed lines show the detection threshold of S/N $\geqslant$ 4. Note the same scales for the light curves and Fourier spectra.

used, it is not clear whether these peaks are due to pulsations of the target.

3. *PN IsWe 1*. The highest, possibly unresolved peak at 49 day^{-1} has S/N = 4.4 and corresponds to a period of about 30 minutes (1764 s). While such pulsation periods are observed in GW Vir stars, observations on a longer time base are necessary for confirmation.
4. *PN Jn 1*. Ciardullo & Bond (1996) observed the star twice, obtaining peaks of maximum amplitude of 2.4 and 4.0 mmag in the Fourier amplitude spectra. They did not detect significant peaks (reaching 99% confidence level) but two candidates, 540.5 and 538.5 μHz (46.70 and 46.53 day^{-1}, respectively), and as a result did not claim the detection of pulsations in the central star of planetary nebula Jn 1. González Pérez et al. (2006) observed the star once and did not find the peaks tentatively detected by Ciardullo & Bond (1996); instead, they found a barely significant peak at 2200 μHz (190.1 day^{-1}). Nevertheless, they claimed discovery of pulsations on that basis but called for more observations to confirm their findings. We observed Jn 1 a total of five times in three different runs, and achieved very good median noise levels of 0.30–0.81 mmag. In none of the runs did we see signs of peaks previously reported or strong peaks occurring in more than one of our own runs (e.g., a peak at 100 day^{-1} with S/N = 4.3 only in McDonald–1 run). We thus conclude that there is no convincing evidence that Jn 1 pulsates and that it requires observations of similar quality to our first McDonald run for eventual confirmation.
5. *RX J0122.9–7521*. RX J0122.9–7521 was observed twice in 2014 December. The light curves and Fourier amplitude spectra are presented in Figure 4. We detected a significant peak in the Fourier amplitude spectra of both nights, located at the same frequency of about 35 day^{-1} and reaching an amplitude of 4–5 mmag. RX J0122.9–7521 was also observed by TESS in Sectors 1, 13, 27, and 28. The same frequency as in our ground-based data is present in the TESS observations (34.78 day^{-1}). With $T_{\rm eff}$ = 180,000 K, that would make RX J0122.9–7521 the hottest known variable/pulsating PG 1159 star. We further discuss this star in Section 10.1.
6. *SDSS J102327.41+535258.7*. One suitable comparison star was used. There are two peaks: 15.7 and 30.4 day^{-1} with S/N of 4.3 and 4.2, which correspond to periods of 92 and 47 minutes (5507 and 2839 s), respectively.
7. *SDSS J105300.24+174932.9*. There are two interesting, but insignificant (S/N = 3.7 and 3.1), peaks at 251.9 and 281.5 day^{-1}, respectively, in the first McDonald run. In the second run, 5 days later, a peak in the same frequency region is present (at about 257 day^{-1}), but due to higher noise, the signal (if real) has only slightly higher amplitude than the highest noise peaks. In the remaining runs we were not able to reach a better noise level than in the first McDonald run, except the GTC run (that was too short).

5.3. Nonpulsators

1. *MCT 0130–1937*. There is a significant low-frequency trend in the light curve (around 10 day^{-1}) that is likely not intrinsic to the star, particularly because there was only one comparison star available that was fainter than the target.
2. *PG 1151–029*. There is a significant low-frequency trend in the light curve, corresponding to a peak around 20 day^{-1}), that is likely caused by sky transparency variations that night.
3. *PG 1520+525*. There is a significant peak (S/N = 4.33) at 725 day^{-1}. To assess whether this peak is real, we calculated differential light curves between the target and two different comparison stars, as well as between these comparison stars, and then computed the Fourier

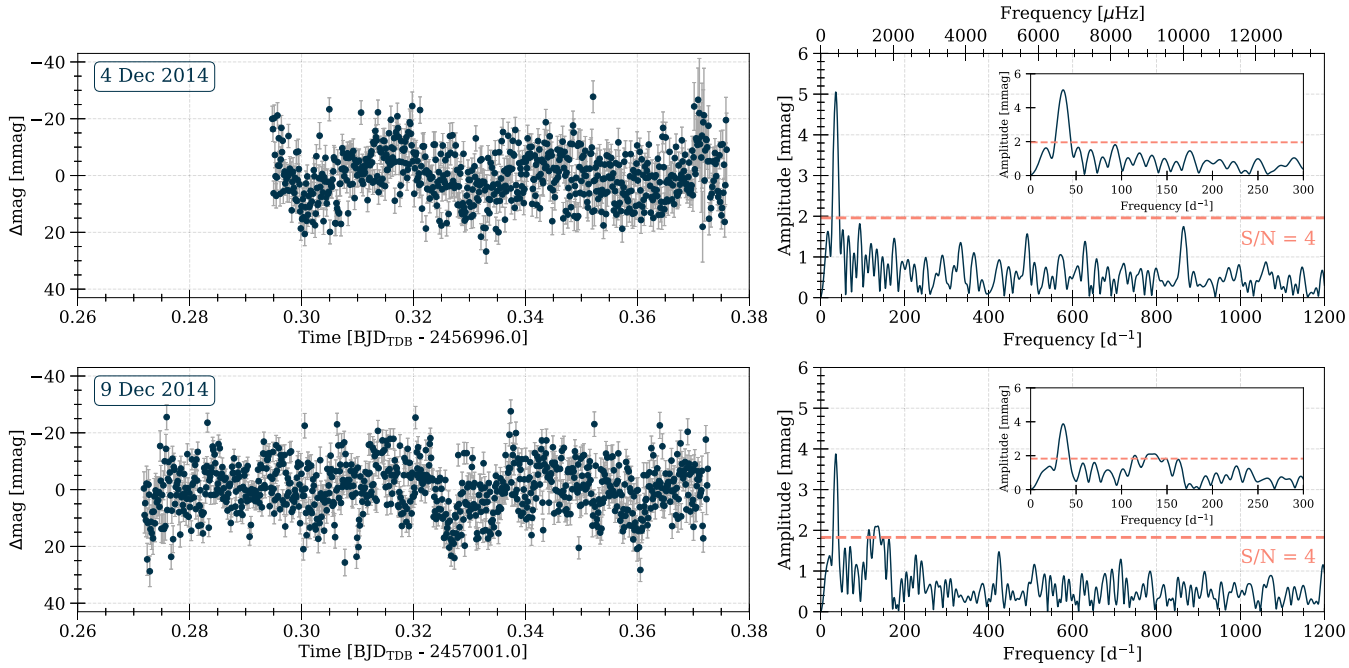

Figure 4. Light curves and Fourier amplitude spectra of two SAAO observing runs on RX J0122.9–7521. The Fourier amplitude spectra were calculated up to the Nyquist frequency but are shown up to 1200 day^{-1}. Insets show a zoomed-in view into the frequency range of the detected variations. Dashed lines show the detection threshold of S/N $\geqslant$ 4. Note the same scales for the light curves and Fourier spectra.

amplitude spectra of these light curves. The aforementioned peak showed up only in the difference of (target–comparison star 1) and not, as expected if the target was variable, also in the difference of (target–comparison star 2). We conclude that, even though formally significant in that differential light curve, this peak is not intrinsic to PG 1520+525.

4. *SDSS J000945.46+135814.4*. The observing run is too short (hence too low frequency resolution) to decide whether the signals around 50 day^{-1} may be intrinsic to the star.
5. *SDSS J093546.53+110529.0*. In the Fourier amplitude spectrum from DK there is a peak around 16 day^{-1} that is due to a low-frequency trend in the light curve and not present in the runs from the other two instruments, one of which has a much lower noise level. We therefore conclude that this signal is not due to pulsations from the target.
6. *SDSS J134341.88+670154.5*. The second run shows a significant low-frequency trend around 20 day^{-1} that is likely due to variable sky conditions and not intrinsic to the star.
7. *SDSS J141556.26+061822.5*. There is a low-frequency peak at 9.46 day^{-1} with S/N = 5.8. This peak corresponds to a period of about 2.5 hr (9000 s), which is too long for GW Vir pulsations. This peak is also present in differential light curves between the target and either of the comparison stars. Therefore, the peak might be intrinsic to the target but of different origin than GW Vir pulsations, e.g., rotation, binarity, or spots.

6. Impurity of GW Vir Instability Strip

Previous observations showed that only about 50% of stars within the GW Vir instability strip pulsate (see, e.g., Figure 2 in Uzundag et al. 2022). With our new results we can redetermine the current occurrence rate for PG 1159 stars. In Table 2 we listed the physical parameters of all known PG 1159 stars with updated information about their variability. For a total of 67 PG 1159 stars, 24 stars are confirmed as pulsating, which corresponds to 36%. Still, the majority of PG 1159 stars within the instability strip are found to be nonpulsators. Sowicka et al. (2021) recently showed that there was a clear separation between N-rich (≈1% N/He) pulsators and N-poor (<0.01% N/He) nonpulsators. We therefore also listed the N abundance, where available, in Table 2. To date, only 26 PG 1159 stars have published N abundances.

7. Properties of All Known PG 1159 Stars

Thanks to the Gaia mission (Gaia Collaboration et al. 2016, 2023), the community received precise measurements of positions and distances of more than one billion stars. For the first time, consistent distance measurements became available for almost the entire sample of PG 1159 stars.[19] In Table 3 we compiled available Gaia DR3 information for PG 1159 stars: identifiers, positions, Gaia G magnitudes, and parallaxes with geometric distances determined by Bailer-Jones et al. (2021). We also list the corresponding reddening $E(B-V)$ at these distances, determined from the 3D reddening map of Green et al. (2018) (`Bayestar17`) using the Python package `dustmaps`. Even though a newer version of `Bayestar` is available (`Bayestar19`; Green et al. 2019), it did not cover the distances of all the stars in our sample; hence, we used the `Bayestar17` reddening map for all but six stars. Those six stars were not covered because of decl. south of −30°. For these cases, we used the 2D dust maps of Schlafly & Finkbeiner (2011) and Schlegel et al. (1998) (SFD), which

[19] With the exception of two stars without sufficient Gaia data, which are listed at the bottom of Table 3.

Table 2
Properties of PG 1159 Stars

Name	$T_{\rm eff}$ (K)	$\log g$ (cm s^{-2})	PN	Puls.	N	BC (mag)	$\log L_\star$ ($L_\odot$)	Ref.
BMP J0739–1418	120,000	6.0	yes	**NOP**	N-poor	−7.269	$3.48^{+0.11}_{-0.12}$	W+2023
FEGU 248–5	160,000	6.5	yes	NVD	N-poor	−8.039	$3.89^{+0.11}_{-0.10}$	W+2023
H1504+65	200,000	8.0	no	**NOP**	N-poor	−8.700	$2.167^{+0.062}_{-0.064}$	W+2004a, WD2005, WR2015, NW2004
HE 1429–1209	160,000	6.0	no	yes	no lit. data	−8.039	$3.46^{+0.11}_{-0.12}$	W+2004b
HS 0444+0453	90,000	7.0	no	**NOP**	no lit. data	−6.429	$1.28^{+0.14}_{-0.16}$	D1999
HS 0704+6153	75,000	7.0	no	**NOP**	N-poor	−5.832	$1.03^{+0.17}_{-0.20}$	DH1998
HS 1517+7403	110,000	7.0	no	**NOP**	N-poor	−7.045	$1.84^{+0.10}_{-0.12}$	DH1998
HS 2324+3944	130,000	6.2	no	yes	no lit. data	−7.460	$3.390^{+0.092}_{-0.084}$	F+2010, S+1999, C+2021
MCT 0130–1937	90,000	7.5	no	**NOP**	N-poor	−6.429	$1.42^{+0.14}_{-0.16}$	W+2004c, WR2014
NGC 246	150,000	5.7	yes	yes	N-poor	−7.855	$3.786^{+0.081}_{-0.084}$	W+2005, CB1996
NGC 650	140,000	7.0	yes	NOP	no lit. data	−7.658	$3.27^{+0.67}_{-0.36}$	NS1995
NGC 6852	150,000	6.0	yes	yes	no lit. data	−7.855	$2.93^{+0.34}_{-0.26}$	K. Werner, GP+2006
NGC 7094	110,000	5.7	yes	yes	N-poor	−7.045	$3.83^{+0.10}_{-0.12}$	F+2010, S+2007
PG 0122+200	80,000	7.5	no	yes	N-rich	−6.043	$1.20^{+0.17}_{-0.19}$	WR2014, F+2007
PG 1144+005	150,000	6.5	no	yes	N-rich	−7.855	$3.13^{+0.10}_{-0.10}$	W+2005, W+2016, S+2021
PG 1151–029	140,000	6.0	no	**NOP**	no lit. data	−7.658	$2.471^{+0.097}_{-0.091}$	W+2004c
PG 1159–035	140,000	7.0	no	yes	N-rich	−7.658	$2.596^{+0.085}_{-0.086}$	W+2005, W+2016, C+2008, O+2022
PG 1424+535	110,000	7.0	no	NOP	N-poor	−7.045	$1.838^{+0.092}_{-0.115}$	W+2005, W+2015
PG 1520+525	150,000	7.5	yes	**NOP**	N-poor	−7.866	$2.591^{+0.081}_{-0.087}$	W+2005, W+2016
PG 1707+427	85,000	7.5	no	yes	N-rich	−6.243	$1.47^{+0.15}_{-0.17}$	W+2005, W+2015, H+2018, K+2004
PN A66 21	140,000	6.5	yes	**NOP**	no lit. data	−7.658	$2.118^{+0.088}_{-0.086}$	W+2004c
PN A66 43	110,000	5.7	yes	yes	N-rich	−7.045	$3.69^{+0.10}_{-0.12}$	F+2010, V+2005
PN A66 72	170,000	6.5	yes	yes	N-rich	−8.212	$3.35^{+0.11}_{-0.12}$	B+2023
PN IsWe 1	90,000	7.0	yes	**NOP**	no lit. data	−6.429	$1.34^{+0.14}_{-0.16}$	D1999
PN Jn 1	150,000	6.5	yes	**NOP**	no lit. data	−7.855	$2.687^{+0.097}_{-0.095}$	RW1995
PN K 1–16	160,000	5.8	yes	yes	no lit. data	−8.039	$3.601^{+0.083}_{-0.088}$	W+2010, G+1987, C+2021
PN Kn 12	170,000	6.5	yes	NVD	no lit. data	−8.212	$3.20^{+0.36}_{-0.28}$	B+2023
PN Kn 61	170,000	6.5	yes	yes	N-rich	−8.212	$3.54^{+0.37}_{-0.27}$	DM+2015, B+2023, S+2023
PN Kn 130	170,000	6.5	yes	NVD	N-poor	−8.212	$3.40^{+0.13}_{-0.13}$	B+2023
PN Lo 3	140,000	6.3	yes	**NOP**	no lit. data	−7.658	$3.08^{+0.15}_{-0.14}$	W+2004c
PN Lo 4	170,000	6.0	yes	yes	N-poor	−8.212	$3.65^{+0.18}_{-0.13}$	W+2010, BM1990
PN Ou 2	170,000	6.5	yes	NVD	no lit. data	−8.212	$2.28^{+0.46}_{-0.22}$	B+2023
PN VV 47	130,000	7.0	yes	NOP	no lit. data	−7.460	$2.04^{+0.11}_{-0.10}$	RW1995
RL 104	80,000	6.0	no	NVD	N-rich	−6.046	$3.17^{+0.15}_{-0.18}$	W+2022
RX J0122.9–7521	180,000	7.5	no	**NOP**	no lit. data	−8.389	$2.958^{+0.067}_{-0.071}$	W+2004c
RX J2117.1+3412	170,000	6.0	yes	yes	no lit. data	−8.212	$3.394^{+0.067}_{-0.071}$	W+2005, V+2002, C+2021
SALT J172411.7–632147	160,000	6.5	no	yes	N-poor	−8.039	$3.01^{+0.11}_{-0.12}$	J+2023
SALT J213742.6–382901	180,000	7.0	no	yes	N-rich	−8.376	$3.04^{+0.17}_{-0.13}$	J+2023
SDSS J000945.46+135814.4	120,000	7.5	no	**NOP**	no lit. data	−7.279	$2.49^{+0.44}_{-0.25}$	K+2016
SDSS J001651.42–011329.3	120,000	5.5	no	**NOP**	no lit. data	−7.269	$3.19^{+0.22}_{-0.18}$	H+2006
SDSS J034917.41–005919.3	90,000	7.5	no	yes	no lit. data	−6.429	$1.33^{+0.19}_{-0.17}$	H+2006, W+2012
SDSS J055905.02+633448.4	11,0000	7.5	no	**NOP**	no lit. data	−7.050	$1.49^{+0.17}_{-0.17}$	W+2014

Table 2
(Continued)

Name	$T_{\rm eff}$ (K)	$\log g$ (cm s^{-2})	PN	Puls.	N	BC (mag)	$\log L_{\star}$ ($L_{\odot}$)	Ref.
SDSS J075415.11+085232.1	12,0000	7.0	no	yes	no lit. data	−7.269	$1.70^{+0.58}_{-0.29}$	W+2014, K+2014
SDSS J075540.94+400918.0	100,000	7.6	no	**NOP**	no lit. data	−6.764	$1.62^{+0.19}_{-0.18}$	H+2006
SDSS J093546.53+110529.0	100,000	7.6	no	**NOP**	no lit. data	−6.764	$1.47^{+0.17}_{-0.17}$	H+2006
SDSS J102327.41+535258.7	110,000	7.6	no	**NOP**	no lit. data	−7.050	$2.15^{+0.23}_{-0.21}$	H+2006
SDSS J105300.24+174932.9	100,000	7.0	no	**NOP**	no lit. data	−6.762	$1.59^{+0.13}_{-0.14}$	W+2014
SDSS J121523.09+120300.8	100,000	7.6	no	**NOP**	no lit. data	−6.764	$1.65^{+0.25}_{-0.21}$	H+2006
SDSS J123930.61+244321.7	100,000	7.5	no	**NOP**	no lit. data	−6.764	$1.64^{+0.25}_{-0.21}$	W+2014
SDSS J134341.88+670154.5	100,000	7.6	no	**NOP**	no lit. data	−6.764	$1.44^{+0.12}_{-0.14}$	H+2006
SDSS J141556.26+061822.5	120,000	7.5	no	**NOP**	no lit. data	−7.279	$1.83^{+0.15}_{-0.13}$	W+2014
SDSS J144734.12+572053.1	100,000	7.6	no	**NOP**	no lit. data	−6.764	$1.58^{+0.19}_{-0.17}$	H+2006
SDSS J152116.00+251437.5	140,000	6.0	no	NOP	no lit. data	−7.658	$3.11^{+0.42}_{-0.29}$	W+2014
SDSS J155610.40+254640.3	100,000	5.3	no	NVD	no lit. data	−6.762	$3.23^{+0.40}_{-0.37}$	R+2016
SDSS J163727.03+485355.2	100,000	7.5	no	NVD	no lit. data	−6.764	$1.86^{+0.39}_{-0.22}$	K+2016
SDSS J191845.01+624343.7	100,000	7.2	no	NOP	no lit. data	−6.762	$1.65^{+0.14}_{-0.15}$	W+2014
SDSS J212531.92–010745.8	100,000	7.5	no	NOP	no lit. data	−6.764	$2.54^{+0.41}_{-0.25}$	K. Werner
Sh 2–68	84,000	7.2	no	**NOP**	no lit. data	−6.205	$1.70^{+0.17}_{-0.16}$	G+2010
Sh 2–78	120,000	7.5	yes	NOP	no lit. data	−7.279	$1.79^{+0.11}_{-0.11}$	D1999
TIC 95332541	100,000	7.5	no	yes	N-poor	−6.764	$2.14^{+0.12}_{-0.13}$	U+2021, R+2023
TIC 333432673	120,000	7.5	no	yes	no lit. data	−7.279	$1.924^{+0.082}_{-0.095}$	U+2021
TIC 403800675	110,000	7.5	no	yes	no lit. data	−7.050	$1.73^{+0.10}_{-0.12}$	U+2022
TIC 1989122424	110,000	7.5	no	yes	no lit. data	−7.050	$1.29^{+0.11}_{-0.13}$	U+2022
WD J070204.29+051420.56	100,000	7.5	no	NVD	N-poor	−6.764	$1.63^{+0.12}_{-0.14}$	R+2023
NGC 6765	⋯	⋯	yes	NVD	no lit. data	⋯	⋯	NS1995
PG 2131+066	95,000	7.5	no	yes	N-rich	⋯	⋯	WR2014, K+1995
RX J0439.8–6809	250,000	8.0	no	NOP	N-poor	⋯	⋯	WR2015

Note. Properties of PG 1159 stars. Bold–this work. NOP—not observed to pulsate; NVD—no variability data available. The last three stars lack either Gaia measurements or $T_{\rm eff}$ and $\log g$ determinations and were excluded from the analysis.

References: BM1990—Bond & Meakes (1990); B+2023—Bond et al. (2023); CB1996—Ciardullo & Bond (1996); C+2008—Costa et al. (2008); C+2021—Córsico et al. (2021); DH1998—Dreizler & Heber (1998); D1999—Dreizler (1999); DM+2015—De Marco et al. (2015); F+2007—Fu et al. (2007); F+2010—Friederich et al. (2010); G+1987—Grauer et al. (1987a); GP+2006—González Pérez et al. (2006); G+2010—Gianninas et al. (2010); H+2006—Hügelmeyer et al. (2006); H+2018—Hoyer et al. (2018); J+2023—Jeffery et al. (2023); K+1995—Kawaler et al. (1995); K+2004—Kawaler et al. (2004); K+2014—Kepler et al. (2014); K+2016—Kepler et al. (2016); NS1995—Napiwotzki & Schoenberner (1995); NW2004—Nagel & Werner (2004); O+2022—Oliveira da Rosa et al. (2022); RW1995—Rauch & Werner (1995); R+2016—Reindl et al. (2016); R+2023—Reindl et al. (2023); S+1999—Silvotti et al. (1999); S+2007—Solheim et al. (2007); S+2021—Sowicka et al. (2021); S+2023—P. Sowicka et al. (2023, in preparation); U+2021—Uzundag et al. (2021); U+2022—Uzundag et al. (2022); V+2002—Vauclair et al. (2002); V+2005—Vauclair et al. (2005); W+2004a—Werner et al. (2004a); W+2004b—Werner et al. (2004b); W+2004c—Werner et al. (2004c); W+2005—Werner et al. (2005); WD2005—Werner & Drake (2005); W+2010—Werner et al. (2010); W+2012—Woudt et al. (2012); W+2014—Werner et al. (2014); WR2014—Werner & Rauch (2014); W+2015—Werner et al. (2015); WR2015—Werner & Rauch (2015); W+2016—Werner et al. (2016); W+2022—Werner et al. (2022a); W+2023—Weidmann et al. (2023).

are equivalent to `Bayestar` in terms of units. We did not take into account the reddening by the surrounding planetary nebulae in the case of PG 1159 stars being the central stars of planetary nebulae. We also listed the renormalized unit weight error (RUWE) coefficient for each star and marked in bold values higher than the canonical 1.4, which might either suggest an unreliable astrometric solution (in a few cases that corresponds with a large parallax error) or be a hint toward binarity. In the final column of Table 3 we put a remark for nonsingle stars (e.g., known or suspected binaries/triples) and a subclass of so-called hybrid-PG 1159 stars (exhibiting traces of hydrogen in the atmosphere).

8. PG 1159 Stars on the Hertzsprung–Russell Diagram

PG 1159 stars plotted in the surface gravity–effective temperature diagram $\log g - \log T_{\rm eff}$ (also called the Kiel diagram) cluster horizontally along the lines of constant $\log g$ and vertically along the lines of constant $\log T_{\rm eff}$ (see Figure 5). The reasons are the current sensitivity of spectroscopic

Table 3
Astrometric Properties of PG 1159 Stars

Name	Gaia ID	R.A. (deg)	Decl. (deg)	Gaia G (mag)	$\varpi_{\rm Gaia}$ (mas)	$\sigma_{\varpi_{\rm Gaia}}/\varpi$ (%)	rgeo (kpc)	$E(B-V)$ (mag)	RUWE	Remarks
BMP J0739–1418	3030005560828868096	114.96064	−14.30718	15.61	0.458 ± 0.042	9	$2.10^{+0.18}_{-0.19}$	0.258 ± 0.021	1.041	
FEGU 248–5	5594969135329315072	115.59902	−32.79746	17.00	0.528 ± 0.052	10	$1.90^{+0.19}_{-0.16}$	0.944[a]	0.997	
H1504+65	1645296216119116928	225.54006	+66.20535	16.29	2.156 ± 0.051	2	$0.47^{+0.12}_{-0.11}$	0.0144 ± 0.0028	1.050	
HE 1429–1209	6324298665725984512	218.08641	−12.38006	16.01	0.441 ± 0.054	12	$2.16^{+0.23}_{-0.22}$	0.101575 ± 0.000099	1.012	
HS 0444+0453	3281864642080410112	071.76880	+04.97804	16.23	2.271 ± 0.062	3	$0.441^{+0.011}_{-0.014}$	0.0473 ± 0.0033	0.985	
HS 0704+6153	1099093607199220096	107.38536	+61.80533	16.98	1.643 ± 0.074	5	$0.615^{+0.033}_{-0.030}$	0.0413 ± 0.0050	0.974	
HS 1517+7403	1697669356564165632	229.19327	+73.86865	16.63	1.319 ± 0.061	5	$0.781^{+0.031}_{-0.037}$	0.0278 ± 0.0024	0.963	
HS 2324+3944	1923253820774422272	351.81644	+40.02323	14.77	0.702 ± 0.034	5	$1.400^{+0.074}_{-0.054}$	0.1343 ± 0.0013	1.112	hybrid
MCT 0130–1937	5140121722033618560	023.16399	−19.36138	15.76	2.395 ± 0.066	3	$0.414^{+0.010}_{-0.011}$	0.0297 ± 0.0021	1.283	
NGC 246	2376592910265354368	011.76385	−11.87198	11.80	1.799 ± 0.079	4	$0.538^{+0.020}_{-0.017}$	0.04481 ± 0.00092	**1.530**	triple
NGC 650	406328443354164480	025.58192	+51.57541	17.42	0.294 ± 0.203	**69**	$3.7^{+2.8}_{-1.5}$	0.1431 ± 0.0073	**1.727**	
NGC 6852	4237745794618477440	300.16337	+01.72801	17.91	0.39 ± 0.12	**30**	$3.0^{+1.1}_{-0.9}$	0.1083 ± 0.0042	1.017	
NGC 7094	1770058865674512896	324.22072	+12.78859	13.52	0.604 ± 0.034	6	$1.607^{+0.092}_{-0.076}$	0.12600 ± 0.00046	0.970	hybrid
PG 0122+200	2786529465445503488	021.34385	+20.29910	16.75	1.641 ± 0.080	5	$0.618^{+0.042}_{-0.032}$	0.0396 ± 0.0018	0.982	
PG 1144+005	3795664157996369024	176.64674	+00.20928	15.16	0.802 ± 0.058	7	$1.220^{+0.085}_{-0.076}$	0.02041 ± 0.00080	1.088	
PG 1151–029	3601781534594624000	178.56280	−03.20143	16.07	1.060 ± 0.063	6	$0.938^{+0.060}_{-0.046}$	0.0382 ± 0.0040	1.044	
PG 1159–035	3600841623951744640	180.44149	−03.76130	14.69	1.691 ± 0.064	4	$0.585^{+0.020}_{-0.021}$	0.0241 ± 0.0031	1.129	
PG 1424+535	1605381435770077312	216.48109	+53.25704	15.88	1.771 ± 0.041	2	$0.566^{+0.012}_{-0.011}$	0.0126 ± 0.0016	1.033	
PG 1520+525	1595941441250636672	230.44399	+52.36779	15.55	1.295 ± 0.041	3	$0.783^{+0.027}_{-0.030}$	0.0256 ± 0.0029	1.045	
PG 1707+427	1355161726346266112	257.19864	+42.68358	16.65	1.402 ± 0.052	4	$0.733^{+0.032}_{-0.026}$	0.0477 ± 0.0012	1.002	
PN A66 21	3163546505053645056	112.26128	+13.24679	15.93	1.689 ± 0.069	4	$0.584^{+0.024}_{-0.021}$	0.0318 ± 0.0013	1.086	
PN A66 43	4488953930631143168	268.38446	+10.62340	14.66	0.458 ± 0.033	7	$2.09^{+0.12}_{-0.11}$	0.1946 ± 0.0087	1.038	hybrid
PN A66 72	1761341417799128320	312.50856	+13.55817	16.01	0.548 ± 0.064	12	$1.84^{+0.18}_{-0.21}$	0.06740 ± 0.00065	1.042	
PN IsWe 1	250358801943821952	057.27473	+50.00410	16.47	2.350 ± 0.057	2	$0.424^{+0.010}_{-0.009}$	0.197 ± 0.045	0.903	
PN Jn 1	2871119705335735552	353.97219	+30.46843	16.00	1.011 ± 0.065	6	$0.982^{+0.071}_{-0.059}$	0.0900 ± 0.0044	1.120	
PN K 1–16	2160562927224840576	275.46708	+64.36482	14.98	0.589 ± 0.035	6	$1.737^{+0.090}_{-0.092}$	0.0388 ± 0.0035	1.102	
PN Kn 12	1823929193070538624	300.84391	+21.59786	18.44	0.33 ± 0.17	**49**	$3.5^{+1.5}_{-1.1}$	0.2839 ± 0.0071	0.961	

Table 3
(Continued)

Name	Gaia ID	R.A. (deg)	Decl. (deg)	Gaia G (mag)	$\varpi_{\rm Gaia}$ (mas)	$\sigma_{\varpi_{\rm Gaia}}/\varpi$ (%)	rgeo (kpc)	$E(B-V)$ (mag)	RUWE	Remarks
PN Kn 61	2052811676760671872	290.41223	+38.31588	18.25	0.14 ± 0.11	**80**	$5.9^{+2.4}_{-1.8}$	0.1327 ± 0.0056	0.986	binary?
PN Kn 130	1941078175572093696	348.27200	+45.43838	16.54	0.497 ± 0.054	11	$2.115^{+0.27}_{-0.27}$	0.1826 ± 0.0022	1.051	
PN Lo 3	5509004952576699904	108.70594	−46.96087	16.74	0.467 ± 0.074	16	$2.10^{+0.30}_{-0.27}$	0.172[a]	**1.787**	
PN Lo 4	5414927915911816704	151.44074	−44.35931	16.59	0.330 ± 0.052	16	$3.06^{+0.60}_{-0.40}$	0.147[a]	1.039	
PN Ou 2	430204780732841600	007.73643	+61.40952	19.27	0.77 ± 0.22	**28**	$1.59^{+0.82}_{-0.38}$	0.3860 ± 0.0072	1.009	
PN VV 47	936605992140011392	119.46507	+53.42137	17.06	1.065 ± 0.079	7	$0.985^{+0.076}_{-0.076}$	0.0371 ± 0.0050	1.008	
RL 104	180006683580428928	067.56196	+40.40398	13.71	0.947 ± 0.021	2	$1.020^{+0.025}_{-0.020}$	0.3071 ± 0.0035	0.964	
RX J0122.9–7521	4637921057358156416	020.72372	−75.35420	15.38	1.196 ± 0.035	3	$0.830^{+0.023}_{-0.024}$	0.053[a]	1.089	
RX J2117.1+3412	1855295171732158080	319.28448	+34.20766	13.02	1.991 ± 0.035	2	$0.4986^{+0.0082}_{-0.0094}$	0.0600 ± 0.0021	0.948	
SALT J172411.7–632147	5910236846008692352	261.04877	−63.36322	16.59	0.585 ± 0.063	11	$1.78^{+0.18}_{-0.19}$	0.065[a]	0.936	
SALT J213742.6–382901	6585736932806500736	324.42712	−38.48355	16.95	0.538 ± 0.087	16	$1.94^{+0.36}_{-0.26}$	0.036[a]	1.061	
SDSS J000945.46+135814.4	2767982864653184640	002.43941	+13.97065	18.07	0.31 ± 0.17	**55**	$2.6^{+1.3}_{-0.7}$	0.0829 ± 0.0041	0.989	
SDSS J001651.42–011329.3	2541718902258404736	004.21425	−01.22487	16.75	0.273 ± 0.079	**29**	$3.36^{+0.81}_{-0.60}$	0.06729 ± 0.00039	0.995	
SDSS J034917.41–005919.3	3251245339191040256	057.32256	−00.98874	17.80	1.15 ± 0.12	10	$0.85^{+0.12}_{-0.08}$	0.1274 ± 0.0061	1.048	
SDSS J055905.02+633448.4	286746241613044096	089.77088	+63.58012	18.59	0.98 ± 0.16	16	$1.06^{+0.17}_{-0.14}$	0.1606 ± 0.0025	1.078	
SDSS J075415.11+085232.1	3145662944130394496	118.56299	+08.87560	19.08	0.57 ± 0.23	**39**	$1.8^{+1.2}_{-0.5}$	0.0321 ± 0.0065	0.961	
SDSS J075540.94+400918.0	920621124593362816	118.92053	+40.15497	17.80	0.95 ± 0.13	13	$1.14^{+0.19}_{-0.13}$	0.0572 ± 0.0041	0.968	
SDSS J093546.53+110529.0	589674614326779136	143.94384	+11.09133	17.75	1.10 ± 0.14	13	$0.96^{+0.13}_{-0.10}$	0.0411 ± 0.0030	0.985	
SDSS J102327.41+535258.7	851812381256776832	155.86423	+53.88297	17.92	0.50 ± 0.11	**23**	$2.03^{+0.47}_{-0.37}$	0.0280 ± 0.0028	0.977	
SDSS J105300.24+174932.9	3982986781494206080	163.25103	+17.82578	16.76	1.429 ± 0.076	5	$0.714^{+0.040}_{-0.034}$	0.0190 ± 0.0016	0.987	
SDSS J121523.09+120300.8	3908341899157118080	183.84614	+12.05020	18.14	0.75 ± 0.14	19	$1.44^{+0.35}_{-0.23}$	0.03492 ± 0.00078	0.928	
SDSS J123930.61+244321.7	3959650269965155584	189.87752	+24.72270	18.30	0.69 ± 0.16	**23**	$1.51^{+0.37}_{-0.26}$	0.0405 ± 0.0090	0.975	
SDSS J134341.88+670154.5	1672427588951276800	205.92436	+67.03180	17.13	1.455 ± 0.055	4	$0.707^{+0.023}_{-0.026}$	0.0284 ± 0.0014	0.937	
SDSS J141556.26+061822.5	3673120627847661184	213.98441	+06.30622	17.44	1.04 ± 0.13	12	$1.00^{+0.14}_{-0.11}$	0.0303 ± 0.0055	1.102	
SDSS J144734.12+572053.1	1613731019696686208	221.89206	+57.34807	18.03	0.835 ± 0.092	11	$1.23^{+0.21}_{-0.13}$	0.0342 ± 0.0082	1.028	
SDSS J152116.00+251437.5	1270099761612163328	230.31665	+25.24375	17.87	0.26 ± 0.11	**43**	$4.4^{+2.1}_{-1.4}$	0.0386 ± 0.0066	1.058	hybrid
SDSS J155610.40+254640.3	1220049614357436544	239.04334	+25.77784	17.91	0.086 ± 0.098	**115**	$7.5^{+3.3}_{-3.0}$	0.0630 ± 0.0077	0.981	binary?

Table 3
(Continued)

Name	Gaia ID	R.A. (deg)	Decl. (deg)	Gaia G (mag)	$\varpi_{\rm Gaia}$ (mas)	$\sigma_{\varpi_{\rm Gaia}}/\varpi$ (%)	rgeo (kpc)	$E(B-V)$ (mag)	RUWE	Remarks
SDSS J163727.03+485355.2	1410694377877399552	249.36262	+48.89866	18.35	0.57 ± 0.11	19	$2.01^{+0.84}_{-0.36}$	0.0261 ± 0.0055	1.018	
SDSS J191845.01+624343.7	2240494910007892608	289.68757	+62.72883	17.58	0.970 ± 0.074	8	$1.111^{+0.101}_{-0.079}$	0.0262 ± 0.0020	1.012	
SDSS J212531.92–010745.8	2686081102494206080	321.38303	−01.12941	17.54	0.35 ± 0.11	**32**	$2.9^{+1.3}_{-0.7}$	0.03730 ± 0.00084	1.034	binary
Sh 2–68	4276328581046447104	276.24337	+00.85976	16.40	2.446 ± 0.059	2	$0.405^{+0.010}_{-0.010}$	0.622 ± 0.048	1.088	hybrid
Sh 2–78	4506484097383382272	285.79198	+14.11631	17.61	1.43 ± 0.10	7	$0.696^{+0.059}_{-0.044}$	0.3160 ± 0.0085	1.045	
TIC 95332541	2997192526074656640	090.68749	−13.85096	15.32	2.593 ± 0.043	2	$0.3845^{+0.0055}_{-0.0050}$	0.0575 ± 0.0049	1.023	
TIC 333432673	2950907725113997312	100.31517	−13.69000	15.21	2.552 ± 0.043	2	$0.3892^{+0.0054}_{-0.0054}$	0.119 ± 0.018	1.093	
TIC 403800675	3486203758501245440	179.36518	−28.06384	16.16	1.875 ± 0.062	3	$0.535^{+0.019}_{-0.018}$	0.0591 ± 0.0040	1.004	
TIC 1989122424	6462935326662402944	319.40996	−55.46694	16.75	1.471 ± 0.062	4	$0.688^{+0.022}_{-0.026}$	0.058[a]	0.987	
WD J070204.29+051420.56	3128765207057429504	105.51783	+5.23904	14.98	3.089 ± 0.053	2	$0.3228^{+0.0053}_{-0.0057}$	0.0472 ± 0.0015	1.091	
NGC 6765	2039515046435901440	287.77732	+30.54545	17.60	0.276 ± 0.078	**28**	$4.0^{+1.5}_{-1.0}$	0.1505 ± 0.0023	1.002	
PG 2131+066	…	…	…	…	…	…	…	…	…	binary
RX J0439.8–6809	…	…	…	…	…	…	…	…	…	

Note. Astrometric properties of PG 1159 stars from Gaia DR3 (Gaia Collaboration et al. 2023). Geometric distances (rgeo) are from Bailer-Jones et al. (2021), and $E(B-V)$ from Bayestar17 (Green et al. 2018) except for targets with decl. south of −30°, where SFD maps (Schlafly & Finkbeiner 2011; Schlegel et al. 1998) were used. Uncertainties in $E(B-V)$ are calculated as half of the difference between values at the 16th and 84th percentile. The last three objects were excluded from the analysis because of the lack of either Gaia measurements or $T_{\rm eff}$ and $\log g$.
[a] Reddening from SFD.

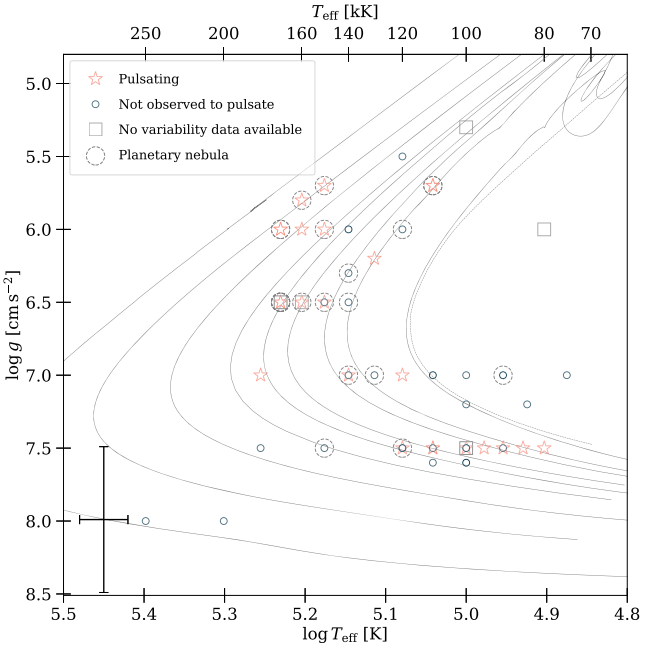

Figure 5. Positions of PG 1159 stars in the surface gravity–effective temperature $\log g - \log T_{\rm eff}$ diagram. Star symbols: pulsating PG 1159 stars; circles: nonvariable; squares: with no reported photometric observations. Stars with planetary nebulae are marked with dashed circles. A typical error bar is shown in the lower left corner. Multiple stars overlap in this diagram, which can be seen as wider and darker borders of symbols. See text for details. Lines represent evolutionary tracks from Miller Bertolami & Althaus (2006): solid lines—VLTP (from left to right, final masses: 0.870, 0.741, 0.664, 0.609, 0.584, 0.565, 0.542, 0.530, 0.515 $M_{\odot}$); single dashed line—LTP (0.512 $M_{\odot}$).

observations (large uncertainties, for some PG 1159 stars even ± 0.5 cm s^{-2} in $\log g$) and availability of advanced model atmospheres for these extremely hot stars, with the latter usually provided in grids with a step of $\log g = 0.5$ cm s^{-2} and $T_{\rm eff} = 10{,}000$ K.

For the discussion in the context of asteroseismology, it is useful to place the PG 1159 stars in the theoretical H-R diagram ($\log L_{\star}/L_{\odot} - \log T_{\rm eff}$). However, this requires the knowledge of stellar luminosities and effective temperatures. Derivation of stellar luminosities is especially challenging because it relies on knowing the total bolometric flux of a given star. There are many ways to tackle this difficult problem. One solution is based on determining the spectral energy distribution by fitting model atmospheres to broadband photometric magnitudes (see, e.g., Uzundag et al. 2022). For such hot stars as PG 1159 stars, the UV photometry and a grid of model atmospheres covering those short wavelengths is essential and, to date, not available for the whole sample of PG 1159 stars.

Another method is to derive the bolometric luminosities, either from mathematical prescriptions or from apparent magnitudes using bolometric corrections (BCs). In the second case, the observed apparent magnitudes are converted to absolute magnitudes in a given passband b using a distance modulus DM (a logarithmic measure of the distance to the star):

$$m_b = M_b + \mathrm{DM}, \tag{1}$$

where m_b is the apparent magnitude and M_b is the absolute magnitude in the passband b. Incorporating the definition of the absolute magnitude gives

$$\mathrm{DM} = m_b - M_b = 5 \log_{10} \frac{d}{(10\ \mathrm{pc})}, \tag{2}$$

where d is distance in parsecs. With the correction for interstellar absorption between the object and observer, the absolute magnitude in a passband b can be derived from

$$M_b = m_b - \mathrm{DM} - A_b, \tag{3}$$

where A_b is the extinction in a passband b. Then, the bolometric magnitude is

$$M_{\rm bol} = M_b + \mathrm{BC}_b, \tag{4}$$

where $M_{\rm bol}$ is absolute bolometric magnitude and BC_b is bolometric correction in a given passband, a quantity dependent not only on the photometric passband used in observations but also on the theoretical stellar spectrum used in calculation of the correction (different sets of effective temperature, surface gravity, and metallicity will give different BC values). In the case of extremely hot stars such as pre-WDs of the PG 1159 type, this requires using models including non-LTE effects. Finally, the absolute bolometric magnitude $M_{\rm bol}$ of a star of a bolometric luminosity $L_{\star}$, referenced to the Sun, is given by

$$-2.5 \log_{10} \frac{L_{\star}}{L_{\odot}} = M_{\rm bol} - M_{\rm bol,\odot}, \tag{5}$$

where $M_{\rm bol,\odot} = 4.74$ is the absolute bolometric magnitude of the Sun and $L_{\odot} = 3.828 \times 10^{33}$ erg s^{-1} is the absolute bolometric luminosity of the Sun.[20]

For WD stars, the first commonly used/tabulated BC values were compiled by Bergeron et al. (1995) for hydrogen- and helium-rich WD model atmospheres, but for a small grid covering surface gravity (only $\log g = 8$ cm s^{-2}) and effective temperature (up to 100,000 K only for DA WDs). This work was expanded by Holberg & Bergeron (2006), who provided an extensive grid for both DA and DB WDs.[21] The latter work is regularly updated online.[22] In the most up-to-date version of the tables, models of Bédard et al. (2020), which include non-LTE effects, are used at the highest effective temperatures. Unfortunately, no BCs have ever been extensively compiled for PG 1159 stars. Some PG 1159 stars had BCs estimated for the purpose of deriving luminosities for asteroseismic modeling (Uzundag et al. 2021 list three previously used values), but no tabulated prescription has ever been provided.

We calculated the luminosities of PG 1159 stars based on currently available data. We used the distances and interstellar reddening values described in Section 7. The reddening for each star was converted to extinction using the reddening law of Fitzpatrick (2004) with $R_V = 3.1$. Gaia magnitudes were

[20] IAU Resolution 2015 B2.

[21] The DA grid covered $T_{\rm eff} = 2500$ K to 150,000 K and $\log g = 7.0$–9.0 cm s^{-2}, while the DB grid covered $T_{\rm eff} = 3250$ K to 150,000 K and $\log g = 7.0$–9.0 cm s^{-2}.

[22] https://www.astro.umontreal.ca/~bergeron/CoolingModels/

converted to V using the following prescription:[23]

$$G - V = -0.02704 + 0.01424(G_{BP} - G_{RP}) - 0.2156(G_{BP} - G_{RP})^2 + 0.01426(G_{BP} - G_{RP})^3. \quad (6)$$

We used tabulated BCs for pure-helium model atmospheres (DB) provided online on the aforementioned website by the Montreal group. As the BC primarily depends on the effective temperature and because there are no BCs computed with proper models for PG 1159 stars, we used those models as the best approach currently available. The tabulated values do not cover surface gravities below $\log g = 7.0$ cm s^{-2}; therefore, the ones for $\log g = 7.0$ cm s^{-2} were used for matching effective temperatures. The values for effective temperatures over 150,000 K were extrapolated to higher effective temperatures for a given $\log g$. The linear extrapolation was done in $\log T_{\rm eff}$ versus BC space using the `interp1d` class from the `scipy` subpackage `interpolate` and "fill_value="extrapolate"," using the available BC values for $T_{\rm eff}$ in the range 75,000–150,000 K for a given $\log g$. Table 2 lists the physical properties and chosen BC values for each PG 1159 star in the sample. Then, the luminosities were calculated following Equations (1)–(5) and are also listed in Table 2 with uncertainties. The errors were propagated the following way: (a) for DM using asymmetric errors from Table 3; (b) for $E(B-V)$ using symmetric errors from Table 3; (c) for BC_V using asymmetric errors adopted as the BC_V values $\pm$10,000 K for each object; (d) for G, G_{BP}, and G_{RP} magnitudes the symmetric errors were calculated as $1.09 \cdot G/(S/N)$, where S/N is roughly `phot_g_mean_flux_over_error`[24] (example for G).

Figure 6 shows positions of PG 1159 stars in the theoretical H-R diagram ($\log L_\star/L_\odot - \log T_{\rm eff}$). For illustration purposes, the blue dotted lines represent theoretical blue edges for $l = 1$ and $l = 2$ modes from Gautschy et al. (2005), but the blue edge is composition dependent ("fuzzy"; Quirion et al. 2007), and with the red dotted lines we show the currently observed red edges.

9. Discussion

The number of pulsating PG 1159 stars increased to 24 objects with our discovery of pulsations in A72. The main observational challenge in the detection or confirmation of variability in those stars lies in two main areas. First, the amplitudes of the g-mode pulsations are quite low. While A72 showed pulsation amplitudes of up to 10 mmag, PG 1144+005, on the other hand, showed a highly variable (between consecutive nights) Fourier spectrum with amplitudes ranging from 3 to 6 mmag (Sowicka et al. 2021). This requires reaching a noise level below 1 mmag for a significant detection (assuming S/N $\geqslant$ 4), which is a challenging task for these faint stars. We were not able to reach noise levels below 1.5 mmag for Longmore 3, SDSS J000945.46+135814.4, SDSS J001651.42–011329.3, SDSS J102327.41+535258.7, and SDSS J144734.12+572053.1. Another challenge is the aforementioned change in amplitude spectra for some stars, between observing seasons or even consecutive nights. It is therefore always possible that the star is observed in a temporary state where the pulsations destructively interfere. We aimed at obtaining more than one run for each star in the sample with a sufficient quality, but this was only possible for eight stars.

Our results allowed us to update the fraction of PG 1159 pulsators in the GW Vir instability strip. While previous works quoted values of about 20%–50%, but including not only PG 1159 stars but also the other stars populating the GW Vir instability strip, we obtain 36% using only stars of PG 1159 spectral type. Our fraction is consistent with previous estimates and shows that only about 1/3 of PG 1159 stars within the GW Vir instability strip are observed to vary.

In this context, it is interesting to see how the variability compares to the nitrogen abundance observed in PG 1159 stars, in light of the nitrogen dichotomy (N-rich pulsators, N-poor nonpulsators, found by Dreizler & Heber 1998) that appears to hold. While the majority of those stars do not have a determination of their atmospheric nitrogen abundance available in the literature, there are a few stars that may not fit this hypothesis. The most recent analysis of the pulsating central star of NGC 246 by Löbling (2018) implies subsolar N abundance. SALT J172411.7–632147 is a N-poor pulsator reported by Jeffery et al. (2023). New spectra of TIC 95332541 analyzed by Reindl et al. (2023) revealed that it is another N-poor pulsator. Longmore 4 is a known pulsator and does not show N in a number of medium-resolution spectra. It is interesting in the context of the outbursts that it exhibits, temporarily changing its spectral type from PG 1159 to [WCE] (Werner et al. 1992; Bond 2014). RL 104 is also an interesting object, as it is N-rich and claimed to have evolved from a binary merger scenario, but to date has not been observed photometrically.

With such a sample tested for variability, we placed the PG 1159 stars in the theoretical H-R diagram. We determined luminosities following the procedure described in Section 8. We plotted them against available evolutionary tracks for PG 1159 stars. In general, very good agreement between the evolutionary tracks and positions of PG 1159 stars was obtained. The majority of the stars are within the evolutionary tracks for typical PG 1159 masses (0.5–0.6 $M_\odot$). Only one star is found beyond 0.87 $M_\odot$—H1504+65. Nevertheless, a few shortcomings of our attempt need to be noted. The distances from Gaia for some stars have large uncertainties owing to large relative errors of parallaxes. In Table 3 we marked 14 stars whose relative parallax errors exceed 20%. Four of them are confirmed or suspected binaries; therefore, their determined positions might be uncertain. It is worth comparing the distances determined using different (independent) methods, e.g., using planetary nebulae line strengths, but this is beyond the scope of this work. Uzundag et al. (2021) quoted available-in-the-literature values of BC for PG 1159 stars for three objects: for PG 1159–035 ($T_{\rm eff} = 140{,}000$ K, $\log g = 7.0$ cm s^{-2}), BC = −7.6; for RX J2117+3142 ($T_{\rm eff} = 170{,}000$ K, $\log g = 6.0$ cm s^{-2}), BC = −7.95; and for PG 2131+066 ($T_{\rm eff} = 95{,}000$ K, $\log g = 7.5$ cm s^{-2}), BC = −6.0. They interpolated those values to obtain BC = −7.05 for TIC 95332541 and TIC 333432673 ($T_{\rm eff} = 120{,}000$, $\log g = 7.5$), assuming only the dependence

[23] Gaia DR3 documentation: https://gea.esac.esa.int/archive/documentation/GDR3/Data_processing/chap_cu5pho/cu5pho_sec_photSystem/cu5pho_ssec_photRelations.html#Ch5.T9. We note that a few objects were slightly outside the range of applicability for this relationship.

[24] https://dc.zah.uni-heidelberg.de/gaia/q3/cone/info#note-e

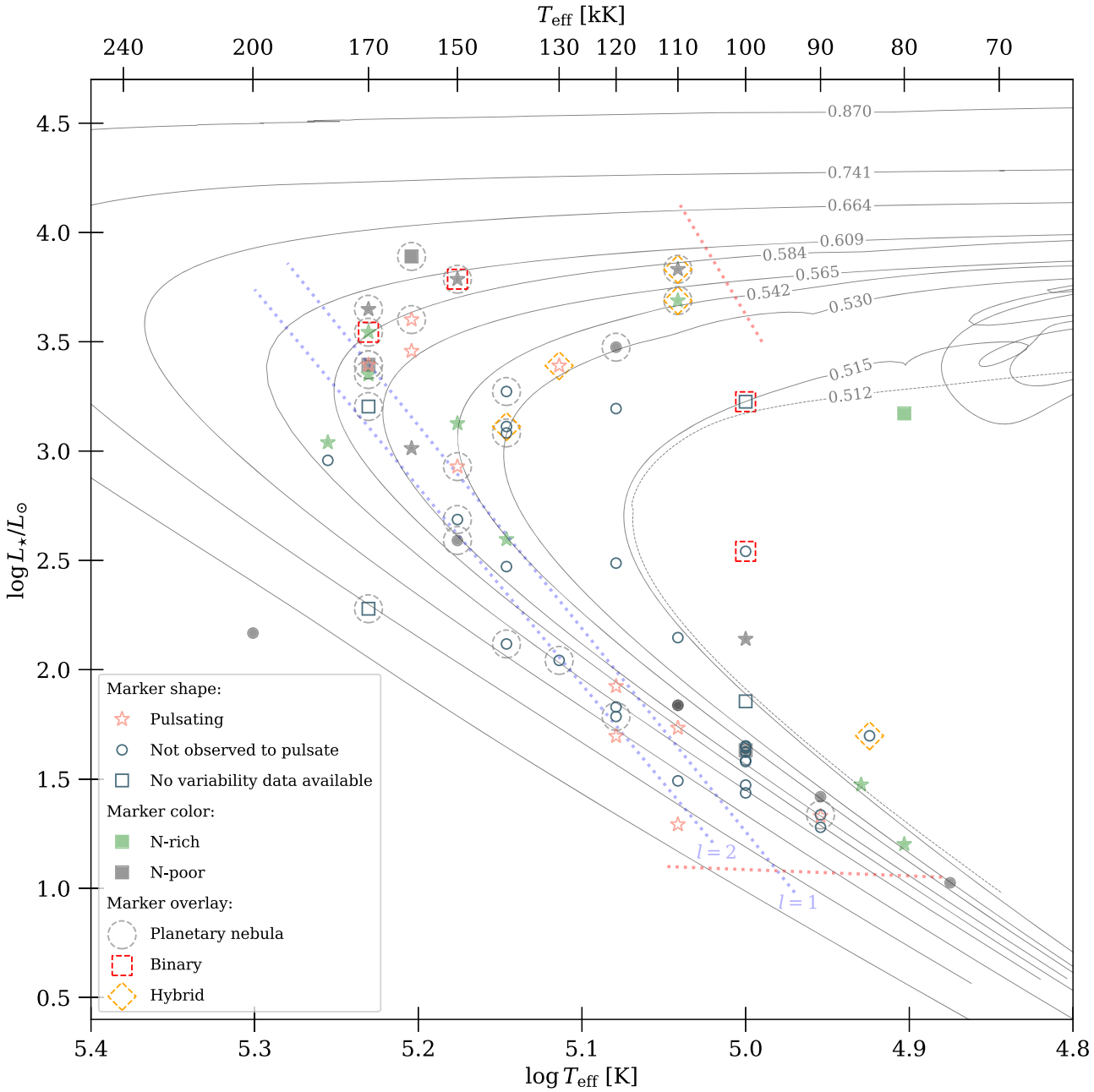

Figure 6. Positions of PG 1159 stars in the theoretical H-R diagram ($\log L_\star/L_\odot$ – $\log T_{\rm eff}$). Star symbols: pulsating PG 1159 stars; circles: nonvariable; squares: with no reported photometric observations. Stars with planetary nebulae are marked with dashed circles. N-rich PG 1159 stars are shown with filled green symbols, while N-poor ones are shown with filled black symbols. Lines represent evolutionary tracks from Miller Bertolami & Althaus (2006): solid lines—VLTP (from left to right, final masses: 0.870, 0.741, 0.664, 0.609, 0.584, 0.565, 0.542, 0.530, 0.515 $M_\odot$); single dashed line—LTP (0.512 $M_\odot$). For illustration purposes, the blue dotted lines represent theoretical blue edges for $l = 1$ and $l = 2$ modes from Gautschy et al. (2005), but the blue edge is composition dependent. The red dotted lines indicate estimated observed red edges, beyond which no GW Vir star has been reported to date.

on the effective temperature. We investigated the difference between tabulated BCs for DA and DB models. For $T_{\rm eff}$ and $\log g$ of PG 1159–035 (the only exact match with tabulated values), we found BCs of −7.964 and −7.658 for DA and DB models, respectively. The value for the DB model atmosphere agrees well with the quoted value of BC = − 7.6. We also checked how the BC value from DB table changes with $\log g$ for a given temperature. For $T_{\rm eff} = 140{,}000$ K and $\log g = 7.0, 7.5, 8.0, 8.5$ cm s^{-2} we obtained BC = −7.658, −7.668, −7.676, −7.681, respectively. Therefore, we do not expect significant interpolation errors in the parameter space of interest.

10. One or Two GW Vir Instability Domains?

The establishment of the PG 1159 spectral class (see, e.g., Werner 1992) occurred subsequently to the discovery of pulsations in PG 1159–035 (McGraw et al. 1979) itself. At the time when the pulsating PG 1159 stars emerged as a new group of pulsators (e.g., Bond et al. 1984), they were considered the hottest subgroup of the helium-rich DO WD stars (Wesemael et al. 1985). For that reason, and for the similarity with the designations of the groups of pulsating WDs already known (DAV and DBV), the PG 1159 pulsators were dubbed "the DOVs."

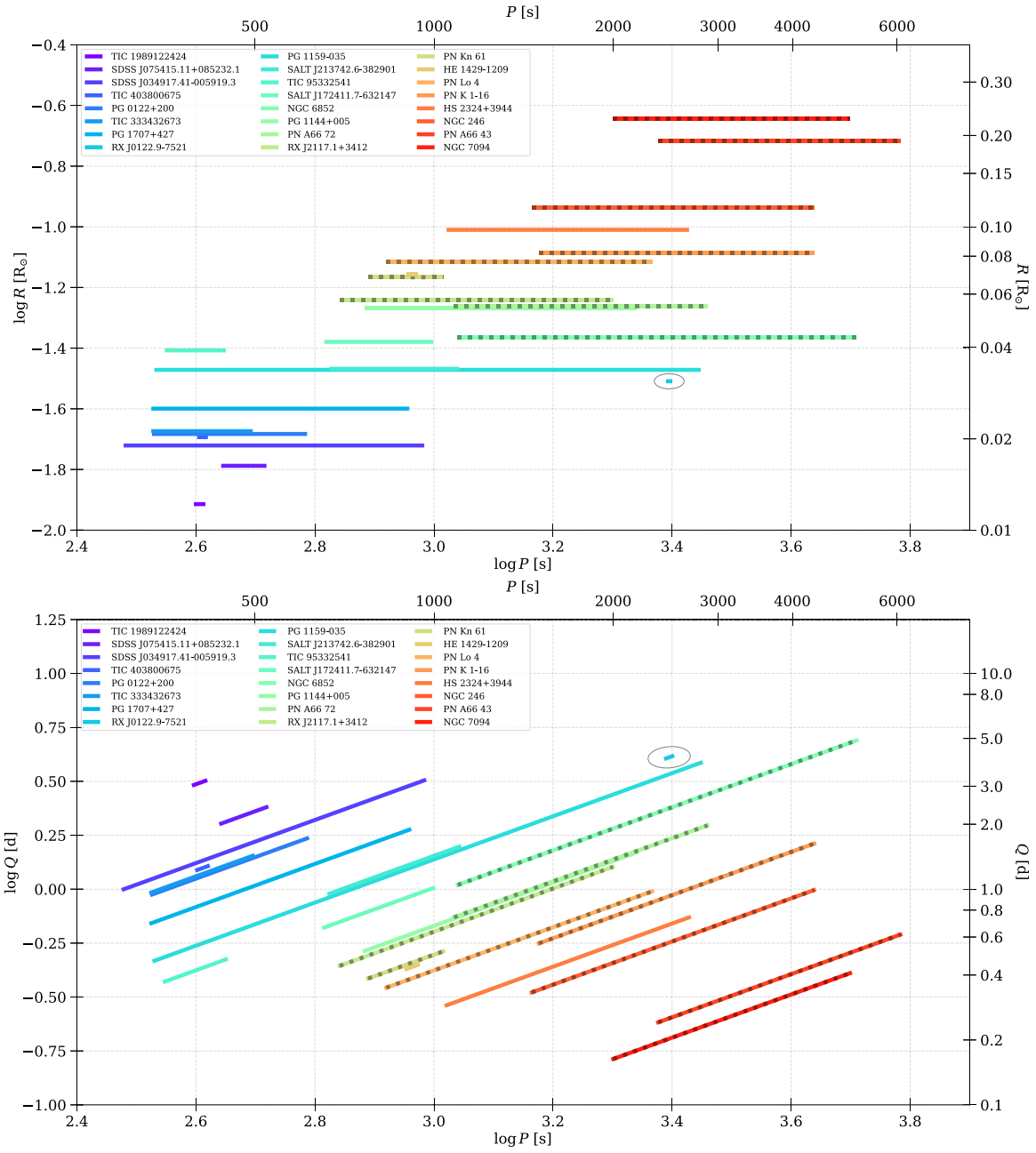

Figure 7. Top: the period ranges of pulsating pre-WD stars (only of PG 1159 spectral type) vs. stellar radius (horizontal bars). Bottom: the period ranges of pulsating pre-WD stars (only of PG 1159 spectral type) vs. pulsation constant (horizontal bars). Objects surrounded by a planetary nebula are denoted with gray dotted bars. The object marked with an ellipse is RX J0122.9–7521 (see Section 10.1).

However, the second pulsating star of the PG 1159 spectral type discovered was located in a planetary nebula (Grauer & Bond 1984), and subsequent searches (e.g., Ciardullo & Bond 1996) revealed several of these "planetary nebula nucleus variables" (PNNVs). Even though it was realized that the "DOVs" were likely just the same type of pulsating stars but in a more advanced evolutionary stage than the "PNNVs," the two groups were historically often separated. The main reason for this separation was that pulsators in one group are surrounded by nebulae whereas the others were not, as well as that one group has significantly longer pulsation periods than the other. Furthermore, theoretical computations (e.g., Córsico et al. 2006; see Figure 6) show that the blue edge of the instability strip intersects with the evolutionary tracks of pre-WD stars in such a way that many of them leave the strip during their evolution and later reenter it, giving the impression of two separated instability regions.

Quirion et al. (2007) and Fontaine & Brassard (2008) argued, mostly on a theoretical basis, that this separation should be dropped and that all hot pulsating pre-WD stars should be called "the GW Vir stars."[25] This was motivated by the fact that the pulsational driving mechanism of all GW Vir stars is the same, that stars with a pure DO spectral type are not known to pulsate,[26] and that not all stars classified as "PNNV" even

[25] GW Vir is the variable star designation of PG 1159–035; Kholopov et al. (1985).

[26] The PG 1159 spectral class had meanwhile been established as a separate group, and we recall that some pulsating pre-WDs are of [WCE] or [WCE/PG 1159] spectral types.

possess a detected planetary nebula. To this it can be added that there are other intrinsically variable central stars of planetary nebulae (e.g., Handler et al. 2013) that do not pulsate at all, which is why a designation "PNNV" is as misleading as "DOV."

Schoenberner & Napiwotzki (1990) showed that some PNNs are spectroscopically indistinguishable from the WDs similar to PG 1159–035 and assigned them all to "PG 1159" type. PG 1159 subclasses introduced by Werner (1992) did not take into account the presence or absence of a nebula, treating the PG 1159 spectral class as a whole. Therefore, not only is the pulsation driving mechanism the same for those stars, but they also share some spectroscopic properties representative of the whole class.

Moreover, the commonly used surface gravity–effective temperature diagram presented in Figure 5 shows that it is impossible to separate the two groups in the $\log g - \log T_{\rm eff}$ plane—stars with planetary nebulae are found throughout the entire GW Vir instability strip. This refutes the argument that the PNNVs usually have much lower surface gravities, as no strict boundary can be placed in such a plane.

In the following, we examine the question whether these two groups are distinct, or should be distinguished, from an observational point of view. The top panel of Figure 7 shows the ranges of pulsation periods observed in pulsating pre-WD stars (of PG 1159 spectral type) versus stellar radius (as derived from Figure 6 and the Stefan–Boltzmann law).

Several things are noteworthy in Figure 7. First of all, there is a clear overlap between the objects with and without a planetary nebula, already suggesting that these two groups are not distinct. Second, an obvious trend, as already noticed by others earlier, is visible, namely that the larger, less evolved objects have longer pulsation periods.

To look into this in some more detail, the bottom panel in Figure 7 compares the pulsation periods with the pulsation constant $Q = P\sqrt{\rho_*/\rho_\odot}$, a measure of the radial overtone of the excited pulsation modes. There is a slight trend such that the longer the pulsation period, the smaller is the pulsation constant. In other words, the more evolved a pulsating pre-WD, the higher radial overtones of the gravity modes are excited. This is consistent with the theoretical expectation that with progressing evolution the pulsational driving region becomes located closer to the stellar surface (see Gautschy et al. 2005).

We therefore conclude that the distinction between "DOVs" and "PNNVs" is, according to current knowledge, artificial and based on selection effects and hence should not be used. All pulsating pre-WD stars oscillating in gravity modes excited by the $\kappa - \gamma$ mechanism due to ionization of carbon and oxygen should henceforth be called "GW Vir stars."

10.1. The Case of RX J0122.9–7521

In Section 5.2 we reported the detection of variability of RX J0122.9–7521 and mentioned that it would be the hottest GW Vir pulsator. However, we are reluctant to claim the firm detection of pulsation for this star, for several reasons.

Although its 41 minute period fits in the range of pulsation periods observed in GW Vir stars (Althaus et al. 2010), we detected only a single period that could therefore in principle be of a different origin, like rotation, binarity, or spots (Reindl et al. 2021). Furthermore, in Figure 7, the period of this star is rather long with respect to stars with similar radii.

RX J0122.9–7521 lies outside the theoretical blue edge of the GW Vir instability strip, and Quirion et al. (2004) unsurprisingly did not find an asteroseismic model with unstable periods in this star. Werner (1995) reported the detection of nitrogen in its spectrum.

In any case, time-resolved spectroscopy or high-S/N photometry would be needed to establish the cause of the variability of RX J0122.9–7521.

11. Summary and Conclusions

We obtained new photometric observations of 29 PG 1159 stars. Over 86 hr of time-series photometry were collected in the years 2014–2022 using telescopes of different sizes, ranging from 1.0 to 10.4 m, and located in both hemispheres. For the majority of stars we achieved a median noise level in Fourier amplitude spectra in the range 0.3–1.0 mmag, which allowed us to discover multiperiodic pulsations in the central star of planetary nebula A72 and variability in RX J0122.9–7521 that could be due to pulsations, binarity, or rotation. Five stars showed interesting peaks but require follow-up observations for confirmation. For the remaining stars our observations put limits on nonvariability. As a result, we derived the fraction of pulsating PG 1159 stars within the GW Vir instability strip: 36%.

In light of the N dichotomy in PG 1159 stars, we compared the new variability results with the literature data on N abundances for those stars and identified objects that could be culprits for this hypothesis: NGC 246, SALT J172411.7–632147, and TIC 95332541 may be N-poor pulsators. Longmore 4 is probably a N-poor pulsator but temporarily changes its spectral type from PG 1159 to [WCE] during outbursts.

Taking advantage of the currently available data, we used distances derived from Gaia parallaxes, interstellar extinction from 3D reddening maps, and BC values from DB tables, to derive luminosities and place the PG 1159 stars in the theoretical H-R diagram. Regardless of the possible caveats of our approach, all stars align well with the PG 1159 evolutionary tracks from Miller Bertolami & Althaus (2006).

Finally, we derived radii and pulsation constants for known pulsators and plotted them against period ranges observed in those stars to further argue against the distinction between "DOVs" and "PNNVs," and we suggested using only the "GW Vir" designation for all stars belonging to that family of pulsating WDs.

12. Author Contributions

P.S. with G.H. and D.J. applied for observing time. P.S., G. H., D.J., J.C., F.v.W., E.P., K.B., L.P., L.S.A., and M.K. observed the targets. D.L.H. extracted single FITS files from data cubes of the SA19+SHOC run. P.S. did the data reduction for all targets except those observed with DK+DFOSC (E.P. reduced those data). P.S. also did photometry and frequency analysis, as well as compiled astrometric parameters of PG 1159 stars and BCs, derived luminosities, placed the sample in the H-R diagrams, and computed radii and pulsation constants. G.H. and D.J. supervised the work. K.W. provided parts of the data included in Table 2. P.S. wrote the text, with contributions from G.H. and feedback from coauthors.

Acknowledgments

We thank the anonymous referee for the valuable comments that improved this manuscript. We thank Philip Short, Nicholas Humphries, and Martha Tabor, who contributed to the observations. This research was supported in part by the National Science Foundation under grant No. NSF PHY-1748958 and by the Polish National Center for Science (NCN) through grants 2015/18/A/ST9/00578 and 2021/43/B/ST9/02972. We acknowledge the support of the Spanish Agencia Estatal de Investigación through grant PID2022-136653NA-I00 funded by MCIN/AEI/10.13039/501100011033 and by "ERDF A way of making Europe". M.K. acknowledges the support from ESA-PRODEX PEA4000127913. This paper uses observations made at the South African Astronomical Observatory (SAAO). Based on observations made with the Gran Telescopio Canarias (GTC), installed in the Spanish Observatorio del Roque de los Muchachos of the Instituto de Astrofísica de Canarias, in the island of La Palma. Based on observations with the Isaac Newton Telescope operated by the Isaac Newton Group at the Observatorio del Roque de los Muchachos of the Instituto de Astrofisica de Canarias on the island of La Palma, Spain. This paper includes data taken at the McDonald Observatory of the University of Texas at Austin. Data were obtained (in part) using the 1.3 m McGraw-Hill Telescope of the MDM Observatory. This work has made use of data from the European Space Agency (ESA) mission Gaia (https://www.cosmos.esa.int/gaia), processed by the Gaia Data Processing and Analysis Consortium (DPAC; https://www.cosmos.esa.int/web/gaia/dpac/consortium). Funding for the DPAC has been provided by national institutions, in particular the institutions participating in the Gaia Multilateral Agreement.

Facilities: GTC (OSIRIS), Radcliffe, Elizabeth (SHOC), ING:Newton (WFC), Struve (ProEM), Danish 1.54m Telescope (DFOSC), McGraw-Hill (Andor).

Software: `Astropy` (Astropy Collaboration et al. 2013, 2018, 2022), `ccdproc` (Craig et al. 2017), `dustmaps` (Green 2018), `matplotlib` (Hunter 2007), `numpy` (Harris et al. 2020), `pandas` (McKinney 2010; pandas development team 2021), `Period04` (Lenz & Breger 2005), `scipy` (Virtanen et al. 2020).

ORCID iDs

Paulina Sowicka https://orcid.org/0000-0002-6605-0268
Gerald Handler https://orcid.org/0000-0001-7756-1568
David Jones https://orcid.org/0000-0003-3947-5946
Ernst Paunzen https://orcid.org/0000-0002-3304-5200
Karolina Bąkowska https://orcid.org/0000-0003-1034-1557
Luis Peralta de Arriba https://orcid.org/0000-0002-3084-084X
Lucía Suárez-Andrés https://orcid.org/0000-0002-0887-1009
Klaus Werner https://orcid.org/0000-0002-6428-2276
Marie Karjalainen https://orcid.org/0000-0003-0751-3231
Daniel L. Holdsworth https://orcid.org/0000-0003-2002-896X

References

Althaus, L. G., Córsico, A. H., Isern, J., & García-Berro, E. 2010, A&ARv, 18, 471
Andersen, J., Andersen, M. I., Klougart, J., et al. 1995, Msngr, 79, 12
Astropy Collaboration, Price-Whelan, A. M., Lim, P. L., et al. 2022, ApJ, 935, 167
Astropy Collaboration, Price-Whelan, A. M., Sipőcz, B. M., et al. 2018, AJ, 156, 123
Astropy Collaboration, Robitaille, T. P., Tollerud, E. J., et al. 2013, A&A, 558, A33
Bailer-Jones, C. A. L., Rybizki, J., Fouesneau, M., Demleitner, M., & Andrae, R. 2021, AJ, 161, 147
Bédard, A., Bergeron, P., Brassard, P., & Fontaine, G. 2020, ApJ, 901, 93
Bergeron, P., Wesemael, F., & Beauchamp, A. 1995, PASP, 107, 1047
Bond, H. E. 2014, AJ, 148, 44
Bond, H. E., Grauer, A. D., Green, R. F., & Liebert, J. W. 1984, ApJ, 279, 751
Bond, H. E., & Meakes, M. G. 1990, AJ, 100, 788
Bond, H. E., Werner, K., Jacoby, G. H., & Zeimann, G. R. 2023, MNRAS, 521, 668
Breger, M., Stich, J., Garrido, R., et al. 1993, A&A, 271, 482
Caldwell, J. A. R., Cousins, A. W. J., Ahlers, C. C., van Wamelen, P., & Maritz, E. J. 1993, SAAOC, 15, 1
Cepa, J. 1998, Ap&SS, 263, 369
Ciardullo, R., & Bond, H. E. 1996, AJ, 111, 2332
Coppejans, R., Gulbis, A. A. S., Kotze, M. M., et al. 2013, PASP, 125, 976
Córsico, A. H., Althaus, L. G., & Miller Bertolami, M. M. 2006, A&A, 458, 259
Córsico, A. H., Althaus, L. G., Miller Bertolami, M. M., González Pérez, J. M., & Kepler, S. O. 2009, ApJ, 701, 1008
Córsico, A. H., Althaus, L. G., Miller Bertolami, M. M., & Kepler, S. O. 2019, A&ARv, 27, 7
Córsico, A. H., Uzundag, M., Kepler, S. O., et al. 2021, A&A, 645, A117
Costa, J. E. S., Kepler, S. O., Winget, D. E., et al. 2008, A&A, 477, 627
Craig, M., Crawford, S., Seifert, M., et al. 2017, astropy/ccdproc: v1.3.0.post1, Zenodo, doi:10.5281/zenodo.1069648
Crowther, P. A., De Marco, O., & Barlow, M. J. 1998, MNRAS, 296, 367
De Marco, O., Long, J., Jacoby, G. H., et al. 2015, MNRAS, 448, 3587
Dreizler, S. 1999, RvMA, 12, 255
Dreizler, S., & Heber, U. 1998, A&A, 334, 618
Fitzpatrick, E. L. 2004, in ASP Conf. Ser. 309, Astrophysics of Dust, ed. A. N. Witt, G. C. Clayton, & B. T. Draine (San Francisco, CA: ASP), 33
Fontaine, G., & Brassard, P. 2008, PASP, 120, 1043
Friederich, F., Rauch, T., Werner, K., Koesterke, L., & Kruk, J. W. 2010, in AIP Conf. Ser. 1273, 17th European White Dwarf Workshop, ed. K. Werner & T. Rauch (Melville, NY: AIP), 231
Fu, J. N., Vauclair, G., Solheim, J. E., et al. 2007, A&A, 467, 237
Gaia Collaboration, Prusti, T., de Bruijne, J. H. J., et al. 2016, A&A, 595, A1
Gaia Collaboration, Vallenari, A., Brown, A. G. A., et al. 2023, A&A, 674, A1
Gautschy, A., Althaus, L. G., & Saio, H. 2005, A&A, 438, 1013
Gianninas, A., Bergeron, P., Dupuis, J., & Ruiz, M. T. 2010, ApJ, 720, 581
González Pérez, J. M., Solheim, J. E., & Kamben, R. 2006, A&A, 454, 527
Grauer, A. D., & Bond, H. E. 1984, ApJ, 277, 211
Grauer, A. D., Bond, H. E., Green, R. F., & Liebert, J. 1987a, in IAU Coll. 95: Second Conf. on Faint Blue Stars, ed. A. G. D. Philip, D. S. Hayes, & J. W. Liebert (Schenectady, NY: L. Davis Press), 231
Grauer, A. D., Bond, H. E., Liebert, J., Fleming, T. A., & Green, R. F. 1987b, ApJ, 323, 271
Green, G. 2018, JOSS, 3, 695
Green, G. M., Schlafly, E., Zucker, C., Speagle, J. S., & Finkbeiner, D. 2019, ApJ, 887, 93
Green, G. M., Schlafly, E. F., Finkbeiner, D., et al. 2018, MNRAS, 478, 651
Green, R. F., & Liebert, J. W. 1979, IAU Colloq. 53: White Dwarfs and Variable Degenerate Stars, ed. H. M. van Horn, V. Weidemann, & M. P. Savedoff, 118
Handler, G., Prinja, R. K., Urbaneja, M. A., et al. 2013, MNRAS, 430, 2923
Harris, C. R., Millman, K. J., van der Walt, S. J., et al. 2020, Natur, 585, 357
Holberg, J. B., & Bergeron, P. 2006, AJ, 132, 1221
Hoyer, D., Rauch, T., Werner, K., & Kruk, J. W. 2018, A&A, 612, A62
Hügelmeyer, S. D., Dreizler, S., Homeier, D., et al. 2006, A&A, 454, 617
Hunter, J. D. 2007, CSE, 9, 90
Jeffery, C. S., Werner, K., Kilkenny, D., et al. 2023, MNRAS, 519, 2321
Kawaler, S. D., O'Brien, M. S., Clemens, J. C., et al. 1995, ApJ, 450, 350
Kawaler, S. D., Potter, E. M., Vučković, M., et al. 2004, A&A, 428, 969
Kepler, S. O., Fraga, L., Winget, D. E., et al. 2014, MNRAS, 442, 2278
Kepler, S. O., Pelisoli, I., Koester, D., et al. 2016, MNRAS, 455, 3413
Kholopov, P. N., Samus, N. N., Kazarovets, E. V., & Perova, N. B. 1985, IBVS, 2681, 1
Lenz, P., & Breger, M. 2005, CoAst, 146, 53
Leuenhagen, U., Koesterke, L., & Hamann, W. R. 1993, AcA, 43, 329
Löbling, L. 2018, Galax, 6, 65
Loumos, G. L., & Deeming, T. J. 1978, Ap&SS, 56, 285
McGraw, J. T., Starrfield, S. G., Liebert, J., & Green, R. 1979, IAU Colloq. 53: White Dwarfs and Variable Degenerate Stars, ed. H. M. van Horn, V. Weidemann, & M. P. Savedoff, 377
McKinney, W. 2010, Proc. of the 9th Python in Science Conf., ed. S. van der Walt & J. Millman, 56

Miller Bertolami, M. M., & Althaus, L. G. 2006, A&A, 454, 845
Miller Bertolami, M. M., Battich, T., Córsico, A. H., Althaus, L. G., & Wachlin, F. C. 2022, MNRAS, 511, L60
Nagel, T., & Werner, K. 2004, A&A, 426, L45
Napiwotzki, R., & Schoenberner, D. 1995, A&A, 301, 545
Oliveira da Rosa, G., Kepler, S. O., Córsico, A. H., et al. 2022, ApJ, 936, 187
pandas development team, 2021 pandas-dev/pandas: Pandas, v1.3.5, Zenodo, doi:10.5281/zenodo.5774815
Quirion, P. O., Fontaine, G., & Brassard, P. 2004, ApJ, 610, 436
Quirion, P. O., Fontaine, G., & Brassard, P. 2007, ApJS, 171, 219
Rauch, T., & Werner, K. 1995, in White Dwarfs, ed. D. Koester & K. Werner (Berlin: Springer), 186
Reindl, N., Geier, S., Kupfer, T., et al. 2016, A&A, 587, A101
Reindl, N., Islami, R., Werner, K., et al. 2023, A&A, 677, A29
Reindl, N., Rauch, T., Werner, K., Kruk, J. W., & Todt, H. 2014, A&A, 566, A116
Reindl, N., Schaffenroth, V., Filiz, S., et al. 2021, A&A, 647, A184
Ricker, G. R., Winn, J. N., Vanderspek, R., et al. 2015, JATIS, 1, 014003
Schlafly, E. F., & Finkbeiner, D. P. 2011, ApJ, 737, 103
Schlegel, D. J., Finkbeiner, D. P., & Davis, M. 1998, ApJ, 500, 525
Schoenberner, D., & Napiwotzki, R. 1990, A&A, 231, L33
Silvotti, R., Dreizler, S., Handler, G., & Jiang, X. J. 1999, A&A, 342, 745
Solheim, J. E., Vauclair, G., Mukadam, A. S., Janulis, R., & Dobrovolskas, V. 2007, A&A, 468, 1057
Sowicka, P., Handler, G., & Jones, D. 2018, MNRAS, 479, 2476
Sowicka, P., Handler, G., Jones, D., & van Wyk, F. 2021, ApJL, 918, L1
Toalá, J. A., Guerrero, M. A., Todt, H., et al. 2015, ApJ, 799, 67
Uzundag, M., Córsico, A. H., Kepler, S. O., et al. 2021, A&A, 655, A27
Uzundag, M., Córsico, A. H., Kepler, S. O., et al. 2022, MNRAS, 513, 2285
Vauclair, G., Fu, J. N., Solheim, J. E., et al. 2011, A&A, 528, A5
Vauclair, G., Moskalik, P., Pfeiffer, B., et al. 2002, A&A, 381, 122
Vauclair, G., Solheim, J. E., & Østensen, R. H. 2005, A&A, 433, 1097
Virtanen, P., Gommers, R., Oliphant, T. E., et al. 2020, NatMe, 17, 261
Walton, N. A., Lennon, D. J., Greimel, R., et al. 2001, INGN, 4, 7
Weidmann, W. A., Werner, K., Ahumada, J. A., Pignata, R. A., & Firpo, V. 2023, A&A, 676, A1
Werner, K. 1992, in The Atmospheres of Early-Type Stars, ed. U. Heber & C. S. Jeffery (Berlin: Springer), 273
Werner, K. 1995, BaltA, 4, 340
Werner, K. 2001, Ap&SS, 275, 27
Werner, K., & Drake, J. J. 2005, A&A, 434, 707
Werner, K., Hamann, W. R., Heber, U., et al. 1992, A&A, 259, L69
Werner, K., & Herwig, F. 2006, PASP, 118, 183
Werner, K., & Rauch, T. 2014, A&A, 569, A99
Werner, K., & Rauch, T. 2015, A&A, 584, A19
Werner, K., Rauch, T., Barstow, M. A., & Kruk, J. W. 2004a, A&A, 421, 1169
Werner, K., Rauch, T., & Kepler, S. O. 2014, A&A, 564, A53
Werner, K., Rauch, T., & Kruk, J. W. 2005, A&A, 433, 641
Werner, K., Rauch, T., & Kruk, J. W. 2010, ApJL, 719, L32
Werner, K., Rauch, T., & Kruk, J. W. 2015, A&A, 582, A94
Werner, K., Rauch, T., & Kruk, J. W. 2016, A&A, 593, A104
Werner, K., Rauch, T., Napiwotzki, R., et al. 2004b, A&A, 424, 657
Werner, K., Rauch, T., Reiff, E., Kruk, J. W., & Napiwotzki, R. 2004c, A&A, 427, 685
Werner, K., Reindl, N., Dorsch, M., et al. 2022a, A&A, 658, A66
Werner, K., Reindl, N., Geier, S., & Pritzkuleit, M. 2022b, MNRAS, 511, L66
Wesemael, F., Green, R. F., & Liebert, J. 1985, ApJS, 58, 379
Woudt, P. A., Warner, B., & Zietsman, E. 2012, MNRAS, 426, 2137